Hindawi
Mathematical Problems in Engineering
Volume 2020, Article ID 7310187, 18 pages
https://doi.org/10.1155/2020/7310187

Research Article

Multipulse Homoclinic Orbits and Chaotic Dynamics of a Reinforced Composite Plate with Carbon Nanotubes

Fengxian An,[1] **Fangqi Chen**,[2,3] **Xiaoxia Bian**,[4] **and Li Zhang**[5]

[1]*Faculty of Mathematics and Physics, Huaiyin Institute of Technology, Huaian 223003, China*
[2]*Department of Mathematics, Nanjing University of Aeronautics and Astronautics, Nanjing 210016, China*
[3]*College of Mathematics and Systems Science, Shandong University of Science and Technology, Qingdao 266590, China*
[4]*School of Mathematics and Physics, Yancheng Institute of Technology, Yancheng 224051, China*
[5]*School of Mathematics and Physics, Anhui University of Technology, Ma'anshan 243002, China*

Correspondence should be addressed to Fengxian An; anfengxian@nuaa.edu.cn

Received 8 January 2020; Revised 6 March 2020; Accepted 7 March 2020; Published 29 April 2020

Academic Editor: Roman Lewandowski

The multipulse homoclinic orbits and chaotic dynamics of a reinforced composite plate with the carbon nanotubes (CNTs) under combined in-plane and transverse excitations are studied in the case of 1 : 1 internal resonance. The method of multiple scales is adopted to derive the averaged equations. From the averaged equations, the normal form theory is applied to reduce the equations to a simpler normal form associated with a double zero and a pair of pure imaginary eigenvalues. The energy-phase method proposed by Haller and Wiggins is utilized to examine the global bifurcations and chaotic dynamics of the CNT-reinforced composite plate. The analytical results demonstrate that the multipulse Shilnikov-type homoclinic orbits and chaotic motions exist in the system. Homoclinic trees are constructed to illustrate the repeated bifurcations of multipulse solutions. In order to verify the theoretical results, numerical simulations are given to show the multipulse Shilnikov-type chaotic motions in the CNT-reinforced composite plate. The results obtained here imply that the motion is chaotic in the sense of the Smale horseshoes for the CNT-reinforced composite plate.

1. Introduction

Carbon nanotubes (CNTs), as a new type of advanced materials, have attracted a lot of attention of researchers. This is because CNTs possess high strength and stiffness with high aspect ratio and low density. Due to these properties of CNTs, a number of studies on the nonlinear vibrations and dynamic responses of CNT-reinforced composite plates have been carried out by many researchers in recent years. By employing an equivalent continuum model, Formica et al. [1] investigated the vibration behaviors of CNT-reinforced composite plates. Zhu et al. [2] presented the bending and free vibration analysis of CNT-reinforced composite plates using the finite element method based on the first-order shear deformation plate theory. In their work, the authors showed the effects of the volume fractions of CNTs and the edge-to-thickness ratios on the bending responses, natural frequencies, and mode shapes of the plates. In addition, Wang and Shen [3] examined the nonlinear dynamic response of CNT-reinforced composite plates resting on elastic foundations in thermal environments. The motion equations were derived based on a higher-order shear deformation theory with a von Kármán-type of kinematic nonlinearity. In [4], a mixed Navier-layerwise differential quadrature method was employed by Malekzadeh and Heydarpour for the free vibration and static response analysis of functionally graded carbon nanotube- (FG-CNT-) reinforced composite laminated plates. Based on the conventional Ritz method accompanied with the Lagrangian multiplier technique, Kiani [5] analyzed the free vibration characteristics of FG-CNT-reinforced composite plates located on point supports. Rafiee et al. [6] applied Galerkin's method to deal with the nonlinear dynamic stability of initially imperfect piezoelectric FG-CNT-reinforced composite plates under combined thermal and electrical loadings. Using the Fourier series expansion and state-space technique, Alibeigloo and Liew [7] investigated the bending behavior of FG-CNT-reinforced composite plates with simply supported edges subjected to thermomechanical loads. Subsequently, this work was extended by Alibeigloo and Emtehani [8] for various boundary conditions by employing the differential quadrature method. Recently, Zhang et al. [9] carried out the analysis of geometrically nonlinear large deformation of triangular FG-CNT-reinforced composite plates using the element-free improved moving least-squares Ritz (IMLS-Ritz) method.

In addition, with the increasing applications of functionally graded materials (FGM) in modern technology, the buckling and vibration analysis of FGM structures began to attract a widespread attention. Thus, many studies on the buckling and vibration analysis of FGM shells have been published in the literature. Zhang and Li [10] discussed the dynamic buckling of FGM truncated conical shells subjected to normal impact loads. Bagherizadeh et al. [11] investigated the mechanical buckling of simply-supported FGM cylindrical shells using third-order shear deformation shell theory. They found that system parameters have great influence on the buckling characteristics of FGM shells. Buckling behavior analysis based on Reddy's high-order shear deformation theory has also been performed by Sun et al. [12] for FGM cylindrical shells subjected to an axial compression in the thermal environment. In recent years, there have been some numerical methods for analyzing the plates and shells. The multiquadric radial basis function (MQ) method was developed and applied by Ferreira [13] to discuss the effects of system parameters on the laminated composite plates. The method of discrete singular convolution (DSC) gives a fast and accurate solution of the mathematical physics and engineering problems. Then, Civalek and his coworkers made a number of remarkable studies using the DSC method; such investigations involved the analysis of composite conical shells and panels [14–16], plates on elastic foundations [17, 18], and so on.

However, in the course of our study, we found that there are only few studies on the global bifurcations and multipulse chaotic dynamics for the CNT-reinforced composite plate. In order to eliminate or suppress large nonlinear vibrations and chaotic motions of the CNT-reinforced composite plate, we should deepen and complete the theoretical analysis on the CNT-reinforced composite plate model, discuss the complex dynamic behaviors, explore the existence conditions of the multipulse Shilnikov-type orbits, and analyze the impact of parameters on the system, so as to ensure the stability and controllability of the CNT-reinforced composite plate. The present work is therefore motivated to examine the global bifurcations and multipulse chaotic dynamics of the CNT-reinforced composite plate considered by Guo and Zhang [19]. The energy-phase method developed by Haller and Wiggins [20] is applied to study the multipulse homoclinic bifurcations and chaotic dynamics for the CNT-reinforced composite plate. In recent decades, two theories that are usually employed to detect the global bifurcations and multipulse Shilnikov-type chaotic dynamics in high-dimensional systems are the energy-phase method [20] and the extended Melnikov method [21]. Also, some researchers have utilized the developed theories to engineering applications, see, for example, [22–29].

Based on the research by Guo and Zhang [19], the averaged equations are obtained for the case of 1 : 1 internal resonance, principal parametric resonance, and 1/2 subharmonic resonance of the CNT-reinforced composite plate. From the averaged equations, the explicit expressions of the 3-order normal form are derived employing the normal form theory. The energy-phase method is utilized to detect the existence of the multipulse Shilnikov-type homoclinic orbits in the CNT-reinforced composite plate. Homoclinic trees are constructed to illustrate the repeated bifurcations of multipulse solutions. In addition, numerical simulations are given to verify the analytical predictions.

The organization of this paper is as follows. In Section 2, we derive the averaged equations and normal form for the CNT-reinforced composite plate. According to the normal form derived in Section 2, the dynamics of the unperturbed system is discussed in Section 3. In Section 4, a detailed dynamic analysis of the perturbed system is presented, and the existence of multipulse homoclinic orbits is confirmed. Numerical simulations are given in Section 5 to show that the chaotic motions can occur in the CNT-reinforced composite plate. A short conclusion is reported in Section 6.

2. Formulation of the Problem

2.1. Equations of Motion and Perturbation Analysis. This paper focuses on studies of the multipulse homoclinic orbits and chaotic dynamics of a four-edge simply-supported CNT-reinforced composite rectangular plate subjected to the in-plane and transverse excitations. The model is shown in Figure 1 [19]. The edge length and width of the plate in the x and y directions are, respectively, a and b, and the thickness is $\tilde{h}$. A Cartesian coordinate system is located in the middle surface of the CNT-reinforced composite rectangular plate. The displacements of an arbitrary point within the plate are u, v, and w in the x, y, and z directions, respectively. The in-plane excitation along the y direction at $x = a$ is given by $P = \tilde{P}_0 - \tilde{P}_1 \cos \Omega_2 t$. The transverse excitation subjecting to the CNT-reinforced composite rectangular plate is of the form $F = F_0 - F_1 \cos \Omega_1 t$.

According to the research by Guo and Zhang [19], the axial and transverse displacement fields at any point for the CNT-reinforced composite plate are given as

$$u(x, y, t) = u_0(x, y, t) + z\varphi_x(x, y, t) - z^3 \frac{4}{3\tilde{h}^2}\left(\varphi_x + \frac{\partial w_0}{\partial x}\right), \tag{1a}$$

$$v(x, y, t) = v_0(x, y, t) + z\varphi_y(x, y, t) - z^3 \frac{4}{3\tilde{h}^2}\left(\varphi_y + \frac{\partial w_0}{\partial y}\right), \tag{1b}$$

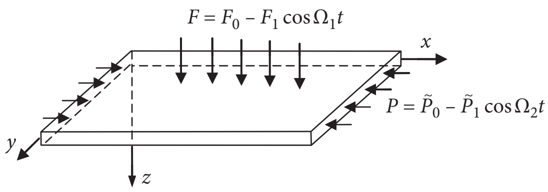

FIGURE 1: The model of a CNT-reinforced composite rectangular plate.

$$w(x, y, t) = w_0(x, y, t), \tag{1c}$$

where u_0, v_0, and w_0 represent the displacements at the midplane of the plate in the x, y, and z directions. φ_x and φ_y denote the rotations of the transverse normal at the midplane about the x and y axes. Employing the von Kármán-type plate theory and in terms of the displacements, the strains $\varepsilon_i\,(i = xx, yy)$ and the curvatures $\gamma_i\,(i = xy, yz, zx)$ in the midplane can be expressed as

$$\begin{aligned}
\varepsilon_{xx} &= \frac{\partial u}{\partial x} + \frac{1}{2}\left(\frac{\partial w}{\partial x}\right)^2, \\
\varepsilon_{yy} &= \frac{\partial v}{\partial y} + \frac{1}{2}\left(\frac{\partial w}{\partial y}\right)^2, \\
\gamma_{xy} &= \frac{1}{2}\left(\frac{\partial u}{\partial x} + \frac{\partial v}{\partial y} + \frac{\partial w}{\partial x}\frac{\partial w}{\partial y}\right), \\
\gamma_{yz} &= \frac{1}{2}\left(\frac{\partial v}{\partial z} + \frac{\partial w}{\partial y}\right), \\
\gamma_{zx} &= \frac{1}{2}\left(\frac{\partial u}{\partial z} + \frac{\partial w}{\partial x}\right).
\end{aligned} \tag{2}$$

The force and moment resultants associated with the strains and curvatures of the plate constitutive equations are

$$\begin{Bmatrix} N_x \\ N_y \\ N_{xy} \end{Bmatrix} = \begin{Bmatrix} A_{11} & A_{12} & A_{16} \\ A_{12} & A_{22} & A_{26} \\ A_{16} & A_{26} & A_{66} \end{Bmatrix} \begin{Bmatrix} \varepsilon_x^{(0)} \\ \varepsilon_y^{(0)} \\ \gamma_{xy}^{(0)} \end{Bmatrix}, \tag{3a}$$

$$\begin{Bmatrix} M_x \\ M_y \\ M_{xy} \end{Bmatrix} = \begin{Bmatrix} D_{11} & D_{12} & D_{16} \\ D_{12} & D_{22} & D_{26} \\ D_{16} & D_{26} & D_{66} \end{Bmatrix} \begin{Bmatrix} \kappa_x^{(0)} \\ \kappa_y^{(0)} \\ \kappa_{xy}^{(0)} \end{Bmatrix} + \begin{Bmatrix} F_{11} & F_{12} & F_{16} \\ F_{12} & F_{22} & F_{26} \\ F_{16} & F_{26} & F_{66} \end{Bmatrix} \cdot \begin{Bmatrix} \kappa_x^{(2)} \\ \kappa_y^{(2)} \\ \kappa_{xy}^{(2)} \end{Bmatrix}, \tag{3b}$$

$$\begin{Bmatrix} P_x \\ P_y \\ P_{xy} \end{Bmatrix} = \begin{Bmatrix} F_{11} & F_{12} & F_{16} \\ F_{12} & F_{22} & F_{26} \\ F_{16} & F_{26} & F_{66} \end{Bmatrix} \begin{Bmatrix} \kappa_x^{(0)} \\ \kappa_y^{(0)} \\ \kappa_{xy}^{(0)} \end{Bmatrix} + \begin{Bmatrix} H_{11} & H_{12} & H_{16} \\ H_{21} & H_{22} & H_{26} \\ H_{16} & H_{26} & H_{66} \end{Bmatrix} \cdot \begin{Bmatrix} \kappa_x^{(2)} \\ \kappa_y^{(2)} \\ \kappa_{xy}^{(2)} \end{Bmatrix}, \tag{3c}$$

$$\begin{Bmatrix} Q_y \\ Q_x \end{Bmatrix} = \begin{Bmatrix} A_{44} & A_{45} \\ A_{45} & A_{55} \end{Bmatrix} \begin{Bmatrix} \gamma_{yz}^{(0)} \\ \gamma_{xz}^{(0)} \end{Bmatrix}, \tag{3d}$$

$$\begin{Bmatrix} R_y \\ R_x \end{Bmatrix} = \begin{Bmatrix} D_{44} & D_{45} \\ D_{45} & D_{55} \end{Bmatrix} \begin{Bmatrix} \gamma_{yz}^{(0)} \\ \gamma_{xz}^{(0)} \end{Bmatrix} + \begin{Bmatrix} F_{44} & F_{45} \\ F_{54} & F_{55} \end{Bmatrix} \begin{Bmatrix} \gamma_{yz}^{(2)} \\ \gamma_{xz}^{(2)} \end{Bmatrix}, \tag{3e}$$

where the coupling matrix B_{ij} and E_{ij} is equal to zero in the stiffness matrix. Then, the nonlinear governing equations of motion for the CNT-reinforced composite plate are obtained as follows [19]:

$$N_{x,x} + N_{xy,y} = I_0\ddot{u}_0 + \left(\tilde{I}_1 - \frac{4}{3\tilde{h}^2}\tilde{I}_3\right)\ddot{\varphi}_x - \frac{4}{3\tilde{h}^2}\tilde{I}_3\frac{\partial\ddot{w}_0}{\partial x}, \tag{4a}$$

$$N_{y,y} + N_{xy,x} = I_0\ddot{v}_0 + \left(\tilde{I}_1 - \frac{4}{3\tilde{h}^2}\tilde{I}_3\right)\ddot{\varphi}_y - \frac{4}{3\tilde{h}^2}\tilde{I}_3\frac{\partial\ddot{w}_0}{\partial y}, \tag{4b}$$

$$\begin{aligned}
&\left(N_{y,y}\frac{\partial w_0}{\partial y} + N_y\frac{\partial^2 w_0}{\partial y^2}\right) + \left(N_{x,x}\frac{\partial w_0}{\partial x} + N_x\frac{\partial^2 w_0}{\partial x^2}\right) + \left(N_{xy,x}\frac{\partial w_0}{\partial y} + N_{xy,y}\frac{\partial w_0}{\partial x} + 2N_{xy}\frac{\partial^2 w_0}{\partial y\partial x}\right) \\
&\quad + \frac{4}{3\tilde{h}^2}\left(P_{x,xx} + 2P_{xy,xy} + P_{y,yy}\right) - \frac{4}{\tilde{h}^2}\left(R_{x,x} + R_{y,y}\right) - \mu\dot{w}_0 + \left(Q_{x,x} + Q_{y,y}\right) + F \\
&= I_0\ddot{w}_0 + \frac{4}{3\tilde{h}^2}\tilde{I}_3\left(\frac{\partial\ddot{u}_0}{\partial x} + \frac{\partial\ddot{v}_0}{\partial y}\right) - \left(\frac{4}{3\tilde{h}^2}\right)^2\tilde{I}_6\left(\frac{\partial^2\ddot{w}_0}{\partial x^2} + \frac{\partial^2\ddot{w}_0}{\partial y^2}\right) + \frac{4}{3\tilde{h}^2}\left(\tilde{I}_4 - \frac{4}{3\tilde{h}^2}\tilde{I}_6\right)\left(\frac{\partial\ddot{\varphi}_x}{\partial x} + \frac{\partial\ddot{\varphi}_y}{\partial y}\right),
\end{aligned} \tag{4c}$$

$$M_{x,x}+M_{xy,y}-\frac{4}{3\tilde{h}^2}P_{x,x}-\frac{4}{3\tilde{h}^2}P_{xy,y}-\left(Q_x-\frac{1}{3\tilde{h}^2}R_x\right)$$
$$=\left(\tilde{I}_1-\frac{4}{3\tilde{h}^2}\tilde{I}_3\right)\ddot{u}_0+\left(\tilde{I}_2-\frac{8}{3\tilde{h}^2}\tilde{I}_4+\left(\frac{4}{3\tilde{h}^2}\right)^2\tilde{I}_6\right)\ddot{\varphi}_x-\frac{4}{3\tilde{h}^2}\left(\tilde{I}_4-\frac{4}{3\tilde{h}^2}\tilde{I}_6\right)\frac{\partial\ddot{w}_0}{\partial x}, \tag{4d}$$

$$M_{y,y}+M_{xy,x}-\frac{4}{3\tilde{h}^2}P_{y,y}-\frac{4}{3\tilde{h}^2}P_{xy,x}-\left(Q_y-\frac{1}{3\tilde{h}^2}R_y\right)$$
$$=\left(\tilde{I}_1-\frac{4}{3\tilde{h}^2}\tilde{I}_3\right)\ddot{v}_0+\left(\tilde{I}_2-\frac{8}{3\tilde{h}^2}\tilde{I}_4+\left(\frac{4}{3\tilde{h}^2}\right)^2\tilde{I}_6\right)\ddot{\varphi}_y-\frac{4}{3\tilde{h}^2}\left(\tilde{I}_4-\frac{4}{3\tilde{h}^2}\tilde{I}_6\right)\frac{\partial\ddot{w}_0}{\partial y}. \tag{4e}$$

Substituting the stress resultants of equations (1a)–(1c), (2), and (3a)–(3e) into equations (4a)–(4e), the governing equations of motion for the CNT-reinforced composite plate in terms of generalized displacements are derived as follows [19]:

$$A_{11}\frac{\partial^2u_0}{\partial x^2}+A_{66}\frac{\partial^2u_0}{\partial y^2}+A_{26}\frac{\partial^2v_0}{\partial y^2}+A_{16}\frac{\partial^2v_0}{\partial x^2}+(A_{12}+A_{66})\frac{\partial^2u_0}{\partial x\partial y}+2A_{16}\frac{\partial^2u_0}{\partial x\partial y}+A_{11}\frac{\partial w_0}{\partial x}\frac{\partial^2w_0}{\partial x^2}+A_{66}\frac{\partial w_0}{\partial x}\frac{\partial^2w_0}{\partial y^2}$$
$$+A_{16}\frac{\partial w_0}{\partial y}\frac{\partial^2w_0}{\partial x^2}+A_{26}\frac{\partial w_0}{\partial y}\frac{\partial^2w_0}{\partial y^2}+2A_{16}\frac{\partial w_0}{\partial x}\frac{\partial^2w_0}{\partial x\partial y}+(A_{12}+A_{66})\frac{\partial w_0}{\partial y}\frac{\partial^2w_0}{\partial x\partial y}=I_0\ddot{u}_0+\left(\tilde{I}_1-\frac{4}{3\tilde{h}^2}\tilde{I}_3\right)\ddot{\varphi}_x-\frac{4}{3\tilde{h}^2}\tilde{I}_3\frac{\partial\ddot{w}_0}{\partial x}, \tag{5a}$$

$$A_{16}\frac{\partial^2u_0}{\partial x^2}+A_{26}\frac{\partial^2u_0}{\partial y^2}+A_{22}\frac{\partial^2v_0}{\partial y^2}+A_{66}\frac{\partial^2v_0}{\partial x^2}+(A_{12}+A_{66})\frac{\partial^2u_0}{\partial x\partial y}+2A_{26}\frac{\partial^2v_0}{\partial x\partial y}+A_{16}\frac{\partial w_0}{\partial x}\frac{\partial^2w_0}{\partial x^2}+A_{26}\frac{\partial w_0}{\partial x}\frac{\partial^2w_0}{\partial y^2}$$
$$+A_{66}\frac{\partial w_0}{\partial y}\frac{\partial^2w_0}{\partial x^2}+A_{22}\frac{\partial w_0}{\partial y}\frac{\partial^2w_0}{\partial y^2}+2A_{26}\frac{\partial w_0}{\partial y}\frac{\partial^2w_0}{\partial x\partial y}+(A_{12}+A_{66})\frac{\partial w_0}{\partial x}\frac{\partial^2w_0}{\partial x\partial y}$$
$$=I_0\ddot{v}_0+\left(\tilde{I}_1-\frac{4}{3\tilde{h}^2}\tilde{I}_3\right)\ddot{\varphi}_y-\frac{4}{3\tilde{h}^2}\tilde{I}_3\frac{\partial\ddot{w}_0}{\partial y}, \tag{5b}$$

$$-c_1^2H_{11}\frac{\partial^4w_0}{\partial x^4}-c_1^2H_{22}\frac{\partial^4w_0}{\partial y^4}+\left[\left(A_{66}+\frac{3}{2}A_{11}\right)\frac{\partial^2w_0}{\partial y^2}+\frac{3}{2}A_{22}\frac{\partial^2w_0}{\partial x^2}+3A_{26}\frac{\partial^2w_0}{\partial x\partial y}\right]\left(\frac{\partial w_0}{\partial x}\right)^2$$
$$-2c_1^2(H_{12}+2H_{66})\frac{\partial^4w_0}{\partial x^2\partial y^2}+\left[\left(A_{66}+\frac{1}{2}A_{11}\right)\frac{\partial^2w_0}{\partial x^2}+\frac{3}{2}A_{22}\frac{\partial^2w_0}{\partial y^2}+3A_{26}\frac{\partial^2w_0}{\partial x\partial y}\right]\left(\frac{\partial w_0}{\partial y}\right)^2-4c_1^2H_{26}\frac{\partial^4w_0}{\partial x\partial y^3}$$
$$-4c_1^2H_{16}\frac{\partial^4w_0}{\partial x^3\partial y}+3A_{16}\frac{\partial w_0}{\partial x}\frac{\partial w_0}{\partial y}\frac{\partial^2w_0}{\partial x^2}+3A_{26}\frac{\partial w_0}{\partial x}\frac{\partial w_0}{\partial y}\frac{\partial^2w_0}{\partial y^2}+(2A_{12}+4A_{66})\frac{\partial^2w_0}{\partial x\partial y}\frac{\partial w_0}{\partial x}\frac{\partial w_0}{\partial y}$$
$$+\left(A_{55}-c_2^2F_{55}+2c_2D_{55}\right)\frac{\partial^2w_0}{\partial x^2}+\left(A_{44}-c_2^2F_{44}+2c_2D_{44}\right)\frac{\partial^2w_0}{\partial y^2}+2\left(A_{45}-c_2^2F_{45}+c_2D_{45}\right)\frac{\partial^2w_0}{\partial x\partial y}$$
$$+\left(A_{26}\frac{\partial u_0}{\partial y}+A_{12}\frac{\partial u_0}{\partial x}+A_{22}\frac{\partial v_0}{\partial y}+A_{26}\frac{\partial v_0}{\partial x}\right)\frac{\partial^2w_0}{\partial y^2}+\left(A_{66}\frac{\partial u_0}{\partial y}+A_{16}\frac{\partial u_0}{\partial x}+A_{26}\frac{\partial v_0}{\partial y}+A_{66}\frac{\partial v_0}{\partial x}\right)\frac{\partial^2w_0}{\partial x\partial y}$$
$$+\left(A_{11}\frac{\partial u_0}{\partial x}+A_{16}\frac{\partial u_0}{\partial y}+A_{12}\frac{\partial v_0}{\partial y}+A_{16}\frac{\partial v_0}{\partial x}\right)\frac{\partial^2w_0}{\partial x^2}+\left[(A_{11}+A_{16})\frac{\partial^2u_0}{\partial x^2}+(A_{26}+A_{22})\frac{\partial^2v_0}{\partial y^2}+A_{16}\frac{\partial^2v_0}{\partial x^2}+A_{66}\frac{\partial^2u_0}{\partial y^2}\right.$$
$$\left.+(A_{12}+A_{66})\frac{\partial^2v_0}{\partial x\partial y}+(A_{16}+A_{66})\frac{\partial^2u_0}{\partial x\partial y}\right]\frac{\partial w_0}{\partial x}+\left[(A_{16}+A_{66})\frac{\partial^2u_0}{\partial x^2}+(A_{22}+A_{26})\frac{\partial^2v_0}{\partial y^2}+A_{66}\frac{\partial^2v_0}{\partial x^2}+A_{26}\frac{\partial^2u_0}{\partial y^2}\right.$$

$$A_{26}\frac{\partial^2 v_0}{\partial x\,\partial y}+(A_{12}+A_{66})\frac{\partial^2 u_0}{\partial x\,\partial y}\Bigg]\frac{\partial w_0}{\partial y}+\left(c_1F_{11}-c_1^2H_{11}\right)\frac{\partial^3\varphi_x}{\partial x^3}+\left(c_1F_{26}-c_1^2H_{26}\right)\frac{\partial^3\varphi_x}{\partial y^3}+c_1\left(3F_{16}-c_1H_{16}\right)\frac{\partial^3\varphi_x}{\partial x^2\partial y}$$
$$+c_1\left(F_{21}+2F_{66}-c_1H_{21}-c_1H_{66}\right)\frac{\partial^3\varphi_x}{\partial x\,\partial y^2}+\left(A_{45}-2c_1D_{45}+c_1^2F_{45}\right)\frac{\partial\varphi_x}{\partial y}+\left(A_{55}-2c_1D_{55}+c_1^2F_{55}\right)\frac{\partial\varphi_x}{\partial x}$$
$$+c_1\left(F_{22}-c_1H_{22}\right)\frac{\partial^3\varphi_y}{\partial y^3}+c_1\left(F_{16}-c_1H_{16}\right)\frac{\partial^3\varphi_y}{\partial x^3}+c_1\left(F_{12}+2F_{66}-c_1H_{21}-c_1H_{66}\right)\frac{\partial^3\varphi_y}{\partial x^2\partial y} \tag{5c}$$
$$+c_1\left(3F_{26}-c_1H_{26}\right)\frac{\partial^3\varphi_y}{\partial x\,\partial y^2}+\left(A_{45}-c_2D_{45}+c_2^2F_{45}\right)\frac{\partial\varphi_y}{\partial x}+\left(A_{44}-c_2D_{44}+c_2^2F_{44}\right)\frac{\partial\varphi_y}{\partial y}+F\cos\Omega_1 t-\mu\dot{w}_0$$
$$=I_0\frac{\partial^2\ddot{w}_0}{\partial t^2}-c_1^2\tilde{I}_6\left(\frac{\partial^2\ddot{w}_0}{\partial x^2}+\frac{\partial^2\ddot{w}_0}{\partial y^2}\right)+c_1\tilde{I}_3\left(\frac{\partial\ddot{u}_0}{\partial x}+\frac{\partial\ddot{v}_0}{\partial y}\right),$$

$$\left(D_{11}-2c_1F_{11}+c_1^2H_{11}\right)\frac{\partial^2\varphi_x}{\partial x^2}+\left(D_{66}-2c_1F_{66}+c_1^2H_{66}\right)\frac{\partial^2\varphi_x}{\partial y^2}+\left(D_{16}-2c_1F_{16}+c_1^2H_{16}\right)\frac{\partial^2\varphi_y}{\partial x^2}$$
$$+\left(D_{22}-2c_1F_{22}+c_1^2H_{22}\right)\frac{\partial^2\varphi_y}{\partial y^2}+\left(D_{21}+D_{16}-2c_1F_{16}-2c_1^2H_{12}\right)\frac{\partial^2\varphi_x}{\partial x\,\partial y}+\left(-A_{55}+2c_2D_{55}-c_2^2F_{55}\right)\varphi_x$$
$$+\left(-A_{45}+2c_2D_{45}-c_2^2F_{45}\right)\varphi_y+\left(c_1^2H_{11}-c_1F_{11}\right)\frac{\partial^3 w_0}{\partial x^3}+\left(c_1^2H_{26}-c_1F_{26}\right)\frac{\partial^3 w_0}{\partial y^3}-\left(c_1^2H_{16}+c_1F_{16}\right)\frac{\partial^2 w_0}{\partial x^2\partial y} \tag{5d}$$
$$+\left(4c_1^2H_{66}-c_1^2H_{12}-2c_1F_{66}-c_1F_{12}\right)\frac{\partial^3 w_0}{\partial x\,\partial y^2}+\left(-A_{55}+2c_2D_{55}-c_2^2F_{55}\right)\frac{\partial w_0}{\partial x}+\left(-A_{45}+2c_2D_{45}-c_2^2F_{45}\right)\frac{\partial w_0}{\partial y}$$
$$=\left(\tilde{I}_2-\frac{4}{3\tilde{h}^2}\tilde{I}_4\right)\ddot{u}_0-\frac{4}{3\tilde{h}^2}\left(\tilde{I}_5-\frac{4}{3\tilde{h}^2}\tilde{I}_7\right)\frac{\partial\ddot{w}_0}{\partial x}+\left(\tilde{I}_3-\frac{8}{3\tilde{h}^2}\tilde{I}_5+\frac{16}{9\tilde{h}^4}\tilde{I}_7\right)\ddot{\varphi}_x,$$

$$\left(D_{16}-2c_1F_{16}+c_1^2H_{16}\right)\frac{\partial^2\varphi_x}{\partial x^2}+\left(D_{26}-2c_1F_{26}+c_1^2H_{26}\right)\frac{\partial^2\varphi_x}{\partial y^2}+\left(D_{66}-2c_1F_{66}+c_1^2H_{66}\right)\frac{\partial^2\varphi_y}{\partial x^2}+\left(D_{22}-2c_1F_{22}+c_1^2H_{22}\right)\frac{\partial^2\varphi_y}{\partial y^2}$$
$$+\left(D_{22}+D_{26}-4c_1F_{16}+2c_1^2H_{12}\right)\frac{\partial^2\varphi_y}{\partial x\,\partial y}+\left(D_{21}+D_{66}-2c_1F_{21}-2c_1F_{66}+c_1^2H_{21}+c_1^2H_{66}\right)\frac{\partial^2\varphi_x}{\partial x\,\partial y}$$
$$-\left(A_{45}-2c_2D_{45}+c_2^2F_{45}\right)\varphi_x-\left(A_{55}-2c_2D_{55}+c_2^2F_{55}\right)\varphi_y+\left(c_1^2H_{16}-c_1F_{16}\right)\frac{\partial^3 w_0}{\partial x^3}+\left(c_1^2H_{22}-c_1F_{22}\right)\frac{\partial^3 w_0}{\partial y^3}$$
$$+\left(2c_1^2H_{66}-c_1^2H_{21}-c_1F_{66}-c_1F_{21}\right)\frac{\partial^3 w_0}{\partial x^2\partial y}-\left(c_1^2H_{26}+c_1F_{26}\right)\frac{\partial^3 w_0}{\partial x\,\partial y^2}-\left(A_{45}-c_2D_{45}+\frac{16}{\tilde{h}^4}F_{45}\right)\frac{\partial w_0}{\partial x}$$
$$-\left(A_{55}-\frac{8}{\tilde{h}^2}D_{55}+\frac{16}{\tilde{h}^4}F_{55}\right)\frac{\partial w_0}{\partial y}=\left(\tilde{I}_2-c_1\tilde{I}_4\right)\ddot{v}_0-c_1\left(\tilde{I}_5-c_1\tilde{I}_7\right)\frac{\partial\ddot{w}_0}{\partial y}+\left(\tilde{I}_3-2c_1\tilde{I}_5+c_1^2\tilde{I}_7\right)\ddot{\varphi}_y, \tag{5e}$$

where μ is the damping coefficient, and all the other coefficients can be found in [19]. The associated boundary conditions for the simply-supported CNT composite plate can be written as

$$\begin{aligned} v=w&=0,\\ \varphi_y&=0,\\ M_{xx}=N_{xy}&=0,\\ x&=0,a, \end{aligned} \tag{6a}$$

$$\begin{aligned} v=w&=0,\\ \varphi_x&=0,\\ M_{yy}=N_{xy}&=0,\\ y&=0,b, \end{aligned} \tag{6b}$$

$$\int_0^{\tilde{h}} N_{xx|x=0\mathrm{d}z}=-\int_0^{\tilde{h}}\left(F_0-F_1\cos\Omega_1 t\right)\mathrm{d}z. \tag{6c}$$

Also, the following nondimensional parameters are introduced:

$$\begin{aligned}
\overline{u}_0 &= \frac{u_0}{a},\\
\overline{v}_0 &= \frac{v_0}{b},\\
\overline{w}_0 &= \frac{w_0}{\widetilde{h}},\\
\overline{\varphi}_x &= \varphi_x,\\
\overline{\varphi}_y &= \varphi_y,\\
\overline{x} &= \frac{x}{a},\\
\overline{y} &= \frac{y}{b},\\
\overline{I}_i &= \frac{1}{L^{i+1}\rho}\widetilde{I}_i,\\
\overline{F} &= \frac{(ab)^{(7/2)}}{E\widetilde{h}^7}F,\\
\overline{P} &= \frac{b^2}{El^3}P,\\
\overline{\mu} &= \frac{1}{\sqrt{\rho E}}\frac{a^2b^2}{\pi^2\widetilde{h}^4}\mu,\\
\overline{T} &= \frac{1}{L}\sqrt{\frac{E}{\rho}}T,\\
\left[\overline{A}_{ij}\right] &= \frac{(ab)^{(1/2)}}{E\widetilde{h}^2}\left[A_{ij}\right],\\
\left[\overline{D}_{ij}\right] &= \frac{(ab)^{(11/2)}}{E\widetilde{h}^4}\left[D_{ij}\right],\\
\left[\overline{F}_{ij}\right] &= \frac{(ab)^{(1/2)}}{E\widetilde{h}^4}\left[D_{ij}\right],\\
\left[\overline{H}_{ij}\right] &= \frac{(ab)^{(1/2)}}{E\widetilde{h}^4}\left[H_{ij}\right],\\
&(i = 1,2,3,4,5,6;\ j = 1,2,3,4,5,6).
\end{aligned} \tag{7}$$

In this paper, our research is focused on the multipulse global bifurcations and chaotic dynamics of the CNT composite plate in its first two modes. Hence, we express w in the following form:

$$w_0 = w_1 \sin\frac{3\pi x}{a}\sin\frac{\pi y}{b} + w_2 \sin\frac{\pi x}{a}\sin\frac{3\pi y}{b}, \tag{8}$$

where w_1 and w_2 are the amplitudes of two modes. The other variables and transverse excitation are given as

$$u_0 = u_1 \sin\frac{3\pi x}{a}\cos\frac{\pi y}{b} + u_2 \sin\frac{\pi x}{a}\cos\frac{3\pi y}{b}, \tag{9a}$$

$$v_0 = v_1 \cos\frac{3\pi x}{a}\sin\frac{\pi y}{b} + v_2 \cos\frac{\pi x}{a}\sin\frac{3\pi y}{b}, \tag{9b}$$

$$\varphi_x = \varphi_1 \cos\frac{3\pi x}{a}\sin\frac{\pi y}{b} + \varphi_2 \cos\frac{\pi x}{a}\sin\frac{3\pi y}{b}, \tag{9c}$$

$$\varphi_y = \varphi_3 \sin\frac{3\pi x}{a}\cos\frac{\pi y}{b} + \varphi_4 \sin\frac{\pi x}{a}\cos\frac{3\pi y}{b}, \tag{9d}$$

$$F = F_1 \sin\frac{3\pi x}{a}\sin\frac{\pi y}{b} + F_2 \sin\frac{\pi x}{a}\sin\frac{3\pi y}{b}. \tag{9e}$$

Then, substituting these expressions into equations (5a)–(5e) and applying the Galerkin integration procedure, we can obtain the displacements u_0, v_0, φ_x, and φ_y with respect to w_0. Consequently, the nonlinear ordinary differential equations of this system in terms of transverse displacements are derived. According to the results of convergence studies given by Hao et al. [30], the dimensionless equations of motion for the CNT-reinforced composite plate in the first two modes are derived as [19]

$$\begin{aligned}
&\ddot{w}_1 + \mu\dot{w}_1 + \omega_1^2 w_1 + a_1 w_1 \cos\Omega_2 t + a_2 w_1^3 + a_3 w_2^3 + a_4 w_1^2 w_2\\
&\quad + a_5 w_1 w_2^2 + a_6 w_1 w_2 + a_7 w_1^2 + a_8 w_2^2 = f_1 \cos\Omega_1 t,
\end{aligned} \tag{10a}$$

$$\begin{aligned}
&\ddot{w}_2 + \mu\dot{w}_2 + \omega_2^2 w_2 + b_1 w_2 \cos\Omega_2 t + b_2 w_1^3 + b_3 w_2^3 + b_4 w_1^2 w_2\\
&\quad + b_5 w_1 w_2^2 + b_6 w_1 w_2 + b_7 w_1^2 + b_8 w_2^2 = f_2 \cos\Omega_1 t,
\end{aligned} \tag{10b}$$

where all the coefficients can be found in [19]. We consider the case of 1 : 1 internal resonance, principal parametric resonance, and 1/2 subharmonic resonance of the CNT-reinforced composite plate, for which the resonant relations are listed as follows:

$$\begin{aligned}
\omega_1 &= \frac{1}{2}\Omega_1 + \widetilde{\varepsilon}\sigma_1,\\
\omega_2 &= \frac{1}{2}\Omega_2 + \widetilde{\varepsilon}\sigma_2,\\
\Omega_1 &= \Omega_2 = \Omega,
\end{aligned} \tag{11}$$

where σ_1 and σ_2 are two detuning parameters. For convenience, we let $\Omega = 2$ in the following analysis. The uniform solutions of equations (10a) and (10b) take the following form:

$$w_n(t,\widetilde{\varepsilon}) = x_{n0}(T_0,T_1) + \widetilde{\varepsilon}x_{n1}(T_0,T_1) + \cdots, \quad n = 1,2, \tag{12}$$

where $T_0 = t$ and $T_1 = \widetilde{\varepsilon}t$. We employ the method of multiple scales to equations (10a) and (10b) and obtain the averaged equations as follows:

$$\dot{x}_1 = -\frac{1}{2}\mu x_1 - \left(\sigma_1 - \frac{1}{4}\alpha_1\right)x_2 - \frac{3}{2}\alpha_2 x_2\left(x_1^2 + x_2^2\right) - \frac{3}{2}\alpha_3 x_4\left(x_3^2 + x_4^2\right) + \frac{1}{2}\alpha_4 x_4\left(x_1^2 - x_2^2\right) - \alpha_4 x_4\left(x_1^2 + x_2^2\right) + \frac{1}{2}\alpha_5 x_2\left(x_3^2 - x_4^2\right) - \alpha_5 x_2\left(x_3^2 + x_4^2\right) - \alpha_4 x_1 x_2 x_3 - \alpha_5 x_1 x_3 x_4, \quad (13a)$$

$$\dot{x}_2 = -\frac{1}{2}\mu x_2 + \left(\sigma_1 + \frac{1}{4}\alpha_1\right)x_1 + \frac{3}{2}\alpha_2 x_1\left(x_1^2 + x_2^2\right) + \frac{3}{2}\alpha_3 x_3\left(x_3^2 + x_4^2\right) + \frac{1}{2}\alpha_4 x_3\left(x_1^2 - x_2^2\right) + \alpha_4 x_3\left(x_1^2 + x_2^2\right) + \frac{1}{2}\alpha_5 x_1\left(x_3^2 - x_4^2\right) + \alpha_5 x_1\left(x_3^2 + x_4^2\right) + \alpha_4 x_1 x_2 x_4 + \alpha_5 x_2 x_3 x_4, \quad (13b)$$

$$\dot{x}_3 = -\frac{1}{2}\mu x_3 - (\sigma_2 - f_0)x_4 - \frac{3}{2}\beta_2 x_2\left(x_1^2 + x_2^2\right) - \frac{3}{2}\beta_3 x_4\left(x_3^2 + x_4^2\right) + \frac{1}{2}\beta_4 x_4\left(x_1^2 - x_2^2\right) - \beta_4 x_4\left(x_1^2 + x_2^2\right) + \frac{1}{2}\beta_5 x_2\left(x_3^2 - x_4^2\right) - \beta_5 x_2\left(x_3^2 + x_4^2\right) - \beta_4 x_1 x_2 x_3 - \beta_5 x_1 x_3 x_4, \quad (13c)$$

$$\dot{x}_4 = -\frac{1}{2}\mu x_4 + (\sigma_2 + f_0)x_3 + \frac{3}{2}\beta_2 x_1\left(x_1^2 + x_2^2\right) + \frac{3}{2}\beta_3 x_3\left(x_3^2 + x_4^2\right) + \frac{1}{2}\beta_4 x_3\left(x_1^2 - x_2^2\right) + \beta_4 x_3\left(x_1^2 + x_2^2\right) + \frac{1}{2}\beta_5 x_1\left(x_3^2 - x_4^2\right) + \beta_5 x_1\left(x_3^2 + x_4^2\right) + \beta_4 x_1 x_2 x_4 + \beta_5 x_2 x_3 x_4, \quad (13d)$$

where $f_0 = (1/4)\beta_1$.

2.2. Computation of Normal Form. In order to study the multipulse chaotic dynamics of the CNT-reinforced composite plate, the first is to reduce equations (13a)–(13d) to a simpler normal form. It is clear that equations (13a)–(13d) possess a trivial zero solution $(x_1, x_2, x_3, x_4) = (0, 0, 0, 0)$ at which the Jacobian matrix can be written as

$$\mathbf{J} = \begin{bmatrix} -\left(\frac{1}{2}\right)\mu & -\sigma_1 + \frac{1}{4}\alpha_1 & 0 & 0 \\ \sigma_1 + \frac{1}{4}\alpha_1 & -\left(\frac{1}{2}\right)\mu & 0 & 0 \\ 0 & 0 & -\left(\frac{1}{2}\right)\mu & -(\sigma_2 - f_0) \\ 0 & 0 & (\sigma_2 + f_0) & -\left(\frac{1}{2}\right)\mu \end{bmatrix}. \quad (14)$$

The characteristic polynomial of Jacobian matrix (14) is

$$|\lambda I - J| = \left[\lambda^2 + \mu\lambda + \frac{1}{4}\mu^2 + \sigma_1^2 - \frac{1}{16}\alpha_1^2\right]\left[\lambda^2 + \mu\lambda + \frac{1}{4}\mu^2 + \sigma_2^2 - f_0^2\right]. \quad (15)$$

It is easy to see that when $\mu = 0$, $\alpha_1 = -4\sigma_1$, and $\sigma_2^2 - f_0^2 > 0$ are satisfied simultaneously, systems (13a)–(13d) have a pair of pure imaginary eigenvalues and one non-semi-simple double zero:

$$\lambda_{1,2} = 0, \qquad \lambda_{3,4} = \pm i\sqrt{\sigma_2^2 - f_0^2}. \quad (16)$$

Setting $\alpha_1 = 2$ and $\sigma = \sigma_1 + (1/4)\alpha_1$ and considering μ, σ, and f_0 as the perturbation parameters, then equations (13a)–(13d) without the perturbation parameters become

$$\dot{x}_1 = x_2 - \frac{3}{2}\alpha_2 x_2\left(x_1^2 + x_2^2\right) - \frac{3}{2}\alpha_3 x_4\left(x_3^2 + x_4^2\right) + \frac{1}{2}\alpha_4 x_4\left(x_1^2 - x_2^2\right) - \alpha_4 x_4\left(x_1^2 + x_2^2\right) + \frac{1}{2}\alpha_5 x_2\left(x_3^2 - x_4^2\right) - \alpha_5 x_2\left(x_3^2 + x_4^2\right) - \alpha_4 x_1 x_2 x_3 - \alpha_5 x_1 x_3 x_4, \quad (17a)$$

$$\dot{x}_2 = \frac{3}{2}\alpha_2 x_1\left(x_1^2 + x_2^2\right) + \frac{3}{2}\alpha_3 x_3\left(x_3^2 + x_4^2\right) + \frac{1}{2}\alpha_4 x_3\left(x_1^2 - x_2^2\right) + \alpha_4 x_3\left(x_1^2 + x_2^2\right) + \frac{1}{2}\alpha_5 x_1\left(x_3^2 - x_4^2\right) + \alpha_5 x_1\left(x_3^2 + x_4^2\right) + \alpha_4 x_1 x_2 x_4 + \alpha_5 x_2 x_3 x_4, \quad (17b)$$

$$\begin{aligned}\dot{x}_3 = {} & -\sigma_2 x_4 - \frac{3}{2}\beta_2 x_2\left(x_1^2 + x_2^2\right) - \frac{3}{2}\beta_3 x_4\left(x_3^2 + x_4^2\right) + \frac{1}{2}\beta_4 x_4\left(x_1^2 - x_2^2\right) - \beta_4 x_4\left(x_1^2 + x_2^2\right) + \frac{1}{2}\beta_5 x_2\left(x_3^2 - x_4^2\right) \\ & - \beta_5 x_2\left(x_3^2 + x_4^2\right) - \beta_4 x_1 x_2 x_3 - \beta_5 x_1 x_3 x_4,\end{aligned} \tag{17c}$$

$$\begin{aligned}\dot{x}_4 = {} & \sigma_2 x_3 + \frac{3}{2}\beta_2 x_1\left(x_1^2 + x_2^2\right) + \frac{3}{2}\beta_3 x_3\left(x_3^2 + x_4^2\right) + \frac{1}{2}\beta_4 x_3\left(x_1^2 - x_2^2\right) + \beta_4 x_3\left(x_1^2 + x_2^2\right) + \frac{1}{2}\beta_5 x_1\left(x_3^2 - x_4^2\right) \\ & + \beta_5 x_1\left(x_3^2 + x_4^2\right) + \beta_4 x_1 x_2 x_4 + \beta_5 x_2 x_3 x_4.\end{aligned} \tag{17d}$$

For the trivial zero solution $(x_1, x_2, x_3, x_4) = (0, 0, 0, 0)$, the Jacobian matrix of equations (17a)–(17d) is evaluated as

$$\mathbf{A} = \begin{bmatrix} 0 & 1 & 0 & 0 \\ 0 & 0 & 0 & 0 \\ 0 & 0 & 0 & -\sigma_2 \\ 0 & 0 & \sigma_2 & 0 \end{bmatrix}. \tag{18}$$

Executing the Maple program designed by Zhang et al. [31] leads to the following 3-order normal form of equations (17a)–(17d):

$$\dot{y}_1 = y_2, \tag{19a}$$

$$\dot{y}_2 = \frac{3}{2}\alpha_2 y_1^3 + \alpha_5 y_1\left(y_3^2 + y_4^2\right), \tag{19b}$$

$$\dot{y}_3 = -\sigma_2 y_4 - \beta_4 y_1^2 y_4 - \frac{3}{2}\beta_3 y_4\left(y_3^2 + y_4^2\right), \tag{19c}$$

$$\dot{y}_4 = \sigma_2 y_3 + \beta_4 y_1^2 y_3 + \frac{3}{2}\beta_3 y_3\left(y_3^2 + y_4^2\right). \tag{19d}$$

Accordingly, the normal form of equations (13a)–(13d) with the perturbation parameters is obtained as

$$\dot{y}_1 = -\frac{1}{2}\mu y_1 + (1 - \sigma) y_2, \tag{20a}$$

$$\dot{y}_2 = \sigma y_1 - \frac{1}{2}\mu y_2 + \frac{3}{2}\alpha_2 y_1^3 + \alpha_5 y_1\left(y_3^2 + y_4^2\right), \tag{20b}$$

$$\dot{y}_3 = -\frac{1}{2}\mu y_3 - (\sigma_2 - f_0) y_4 - \beta_4 y_1^2 y_4 - \frac{3}{2}\beta_3 y_4\left(y_3^2 + y_4^2\right), \tag{20c}$$

$$\dot{y}_4 = (\sigma_2 + f_0) y_3 - \frac{1}{2}\mu y_4 + \beta_4 y_1^2 y_3 + \frac{3}{2}\beta_3 y_3\left(y_3^2 + y_4^2\right). \tag{20d}$$

Letting

$$\begin{aligned} y_3 &= I\cos\phi, \\ y_4 &= I\sin\phi, \end{aligned} \tag{21}$$

we have

$$\dot{y}_1 = -\frac{1}{2}\mu y_1 + (1 - \sigma) y_2, \tag{22a}$$

$$\dot{y}_2 = \sigma y_1 - \frac{1}{2}\mu y_2 + \frac{3}{2}\alpha_2 y_1^3 + \alpha_5 y_1 I^2, \tag{22b}$$

$$\dot{I} = -\frac{1}{2}\mu I + f_0 I \sin 2\phi, \tag{22c}$$

$$I\dot{\phi} = \sigma_2 I + \beta_4 y_1^2 I + \frac{3}{2}\beta_3 I^3 + f_0 I \cos 2\phi. \tag{22d}$$

We then construct the following transformation to find the unfolding of equations (22a)–(22d):

$$\begin{bmatrix} y_1 \\ y_2 \end{bmatrix} = \frac{\sqrt{|\alpha_5|}}{\sqrt{|\beta_4|}} \begin{bmatrix} 1 - \sigma & 0 \\ \frac{1}{2}\mu & 1 \end{bmatrix} \begin{bmatrix} z_1 \\ z_2 \end{bmatrix}. \tag{23}$$

Substituting equation (23) into equations (22a)–(22d) and canceling the nonlinear terms including parameter σ, the unfolding of equations (22a)–(22d) can be derived as

$$\dot{z}_1 = z_2, \tag{24a}$$

$$\dot{z}_2 = -\overline{\mu} z_1 - \mu u_2 + \eta z_1^3 + \alpha_5 z_1 I^2, \tag{24b}$$

$$\dot{I} = -\frac{1}{2}\mu I + f_0 I \sin 2\phi, \tag{24c}$$

$$I\dot{\phi} = \sigma_2 I + \alpha_5 z_1^2 I + \frac{3}{2}\beta_3 I^3 + f_0 I \cos 2\phi, \tag{24d}$$

where $\overline{\mu} = (1/4)\mu^2 - \sigma(1 - \sigma)$ and $\eta = (3\alpha_2\alpha_5/2\beta_4)$. Introduce the scale transformations

$$\begin{aligned} \mu &\longrightarrow \varepsilon\mu, \\ f_0 &\longrightarrow \varepsilon f_0. \end{aligned} \tag{25}$$

Then, equation (24a)–(24d) can be expressed as the Hamilton form with perturbations:

$$\dot{z}_1 = \frac{\partial H}{\partial z_2} + \varepsilon g^{z_1} = z_2, \tag{26a}$$

$$\dot{z}_2 = -\frac{\partial H}{\partial z_1} + \varepsilon g^{z_2} = -\overline{\mu} z_1 + \eta z_1^3 + \alpha_5 z_1 I^2 - \varepsilon\mu z_2, \tag{26b}$$

$$\dot{I} = \frac{\partial H}{\partial \phi} + \varepsilon g^I + \varepsilon f_0 I \sin 2\phi = -\frac{1}{2}\varepsilon\mu I + \varepsilon f_0 I \sin 2\phi, \tag{26c}$$

$$\begin{aligned} I\dot{\phi} &= -\frac{\partial H}{\partial I} + \varepsilon g^{\phi} + \varepsilon f_0 I \cos 2\phi \\ &= \sigma_2 I + \alpha_5 z_1^2 I + \frac{3}{2}\beta_3 I^3 + \varepsilon f_0 I \cos 2\phi. \end{aligned} \tag{26d}$$

The Hamiltonian function H takes the form

$$\begin{aligned} H &= \frac{1}{2}z_2^2 + \frac{1}{2}\overline{\mu}z_1^2 - \frac{1}{4}\eta z_1^4 - \frac{1}{2}\alpha_5 z_1^2 I^2 - \frac{1}{2}\sigma_2 I^2 - \frac{3}{8}\beta_3 I^4, \\ g^{z_1} &= 0, \\ g^{z_2} &= -\mu z_2, \\ g^{I} &= -\frac{1}{2}\mu I, \\ g^{\phi} &= 0. \end{aligned} \tag{27}$$

3. Dynamics of the Unperturbed System

Setting $\varepsilon = 0$ in equations (26a)–(26d) results in the completely integrable equations defined as the unperturbed system. Hence, we will now study the nonlinear dynamics of the following unperturbed system:

$$\dot{z}_1 = z_2, \tag{28a}$$

$$\dot{z}_2 = -\overline{\mu}z_1 + \eta z_1^3 + \alpha_5 z_1 I^2, \tag{28b}$$

$$\dot{I} = 0, \tag{28c}$$

$$I\dot{\phi} = \sigma_2 I + \alpha_5 z_1^2 I + \frac{3}{2}\beta_3 I^3. \tag{28d}$$

Consider the first two equations of systems (28a)–(28d):

$$\dot{z}_1 = z_2, \tag{29a}$$

$$\dot{z}_2 = -\overline{\mu}z_1 + \eta z_1^3 + \alpha_5 z_1 I^2. \tag{29b}$$

Note that homoclinic bifurcations occur in systems (29a) and (29b) for $\eta < 0$. Also, when $\overline{\mu} - \alpha_5 I^2 > 0$, we can obtain that systems (29a) and (29b) have only the trivial zero solution $(z_1, z_2) = (0, 0)$ being a center. On a curve expressed by $\overline{\mu} = \alpha_5 I^2$, that is,

$$I_1 = \left[\frac{(1/4)\mu^2 - \sigma(1-\sigma)}{\alpha_5}\right]^{(1/2)}, \tag{30}$$

three solutions bifurcate from the trivial zero solution through a pitchfork bifurcation denoted by $q_0(I) = (0, 0)$ and $q_{\pm}(I) = (B, 0)$, respectively, where

$$B = \pm\left[\frac{(1/4)\mu^2 - \sigma(1-\sigma) - \alpha_5 I^2}{\eta}\right]^{(1/2)}. \tag{31}$$

For all $I \in [I_1, +\infty)$, systems (29a) and (29b) possess one hyperbolic saddle point $q_0(I)$ connected to itself by a pair of homoclinic orbits, $z_{\pm}^h(T_1, I)$, that is, $\lim_{T_1 \longrightarrow \pm\infty} z_{\pm}^h(T_1, I) = q_0(I)$. Therefore, the set defined by

$$M = \{(z, I, \phi) \mid z = q_0(I), I > I_1, 0 \le \phi \le 2\pi\}, \tag{32}$$

is a two-dimensional invariant manifold in the full four-dimensional phase space. Based on the analysis given by Haller and Wiggins [20], we know that the two-dimensional invariant manifold M is normally hyperbolic and contains three-dimensional stable and unstable manifolds. Let $W^s(M)$ and $W^u(M)$, respectively, denote the stable and unstable manifolds. The existence of the homoclinic orbit in systems (29a) and (29b) to $q_0(I) = (0, 0)$ means that $W^s(M)$ and $W^u(M)$ intersect nontransversally along a three-dimensional homoclinic manifold Γ described as follows:

$$\begin{aligned} \Gamma = \Big\{ &(z, I, \phi) \mid z = z_{\pm}^h(T_1, I), I > I_1, \phi = \frac{1}{I}\int_0^{T_1} D_I H \\ &\cdot \left(z_{\pm}^h(s, I), I\right) \mathrm{d}s + \phi_0 \Big\}, \end{aligned} \tag{33}$$

where $D_I H(z, I) = -(\partial H/\partial I)$. Letting $\xi_1 = -\overline{\mu} + \alpha_5 I^2$, $\delta_1 = -\eta$, systems (29a) and (29b) can be rewritten as

$$\dot{z}_1 = z_2, \tag{34a}$$

$$\dot{z}_2 = \xi_1 z_1 - \delta_1 z_1^3. \tag{34b}$$

The Hamiltonian for Hamilton systems (34a) and (34b) is

$$\overline{H}(z_1, z_2) = \frac{1}{2}z_2^2 - \frac{1}{2}\xi_1 z_1^2 + \frac{1}{4}\delta_1 z_1^4. \tag{35}$$

When $\overline{H} = 0$, there is a homoclinic loop Γ^0 formed by one saddle point $q_0(I)$ and a pair of homoclinic orbits $z_{\pm}(T)_1$. Using equations (34a) and (34b) and (35), the analytical expressions for the homoclinic orbits of (34a) and (34b) are then obtained as

$$z_1(T_1) = \pm\sqrt{\frac{2\xi_1}{\delta_1}}\operatorname{sech}\left(\sqrt{\xi_1}\,T_1\right), \tag{36a}$$

$$z_2(T_1) = \mp\frac{\sqrt{2}\xi_1}{\sqrt{\delta_1}}\tanh\left(\sqrt{\xi_1}\,T_1\right)\operatorname{sech}\left(\sqrt{\xi_1}\,T_1\right). \tag{36b}$$

We now consider the dynamics of the unperturbed system of (26a) and (26d) restricted to M given by

$$\dot{I} = 0, \tag{37a}$$

$$I\dot{\phi} = \sigma_2 I + \alpha_5 I q_0^2(I) + \frac{3}{2}\beta_3 I^3 = D_I H(q_0(I), I), \quad I > I_1. \tag{37b}$$

If the condition $D_I H(q_0(I), I) \ne 0$ holds, I = constant is a periodic orbit, and if $D_I H(q_0(I), I) = 0$, I = constant is a circle of fixed points. A value of $I \in [I_1, +\infty)$ for which $D_I H(q_0(I), I) = 0$ is referred to as a resonant value I, and these fixed points are identified as resonant fixed points. A resonant value is denoted by I_r such that

$$D_I H(q_0(I), I) = \sigma_2 I + \frac{3}{2}\beta_3 I^3 = 0. \tag{38}$$

Thus, the resonant value I_r is derived as

$$I_r = \sqrt{-\frac{2\sigma_2}{3\beta_3}}. \tag{39}$$

For $I = I_r$, the phase shift $\Delta\phi$ can be defined as

$$\Delta\phi = \phi(+\infty, I_r) - \phi(-\infty, I_r), \tag{40}$$

which will be used in subsequent studies to determine the condition under which the multipulse Shilnikov-type homoclinic orbits may exist. Substituting the first equations of (36a) and (36b) into the fourth equations of (28a)–(28d) leads to

$$\dot{\phi} = \sigma_2 + \frac{3}{2}\beta_3 I^2 + \frac{2\alpha_5\xi_1}{\delta_1}\operatorname{sech}^2\left(\sqrt{\xi_1}\,T_1\right). \tag{41}$$

After integration, we obtain

$$\phi(T_1) = \left(\sigma_2 + \frac{3}{2}\beta_3 I^2\right)T_1 + \frac{2\alpha_5\sqrt{\xi_1}}{\delta_1}\tanh\left(\sqrt{\xi_1}\,T_1\right) + \phi_0. \tag{42}$$

Accordingly, the phase shift is also obtained as

$$\triangle\phi = \left[\frac{4\alpha_5\sqrt{\xi_1}}{\delta_1}\right]_{I=I_r} = -\frac{4\alpha_5}{\eta}\sqrt{-\frac{1}{4}\mu^2 + \sigma(1-\sigma) + \alpha_5 I_r^2}. \tag{43}$$

4. Dynamics of the Perturbed System

After obtaining the detailed properties of the subspace (z_1, z_2) for systems (28a)–(28d), the next step is to examine the effects of small perturbation terms $(0 < \varepsilon \ll 1)$ on systems (28a)–(28d). The energy-phase method developed by Haller and Wiggins [20] is utilized to determine the existence of multipulse orbits and chaotic dynamics in the CNT-reinforced composite rectangular plate.

4.1. The Case of Dissipative Perturbations. We start by considering the influence of such small perturbations on manifold M. Based on the research by Haller and Wiggins [20], we know that the manifold M is invariant for small nonzero ε. Therefore, the perturbed annulus M_ε is taken to be the same as M. That is,

$$M_\varepsilon = \left\{(z, I, \phi) \mid z = q_0(I), I > I_1, 0 \le \phi \le 2\pi\right\}. \tag{44}$$

In order to study the dynamic behaviors of the perturbed vector field restricted to M_ε near the resonance $I = I_r$, we now introduce the following scale transformations:

$$\begin{aligned} I &= I_r + \sqrt{\varepsilon}h, \\ \tau &= \sqrt{\varepsilon}T_1. \end{aligned} \tag{45}$$

The last two equations of (26a)–(26d) then become

$$h' = -\frac{1}{2}\mu I_r + f_0 I_r \sin 2\phi + \sqrt{\varepsilon}\left(-\frac{1}{2}\mu h + f_0 h \sin 2\phi\right), \tag{46a}$$

$$\phi' = 3\beta_3 I_r h + \sqrt{\varepsilon}\left(\frac{3}{2}\beta_3 h^2 + f_0 \cos 2\phi\right), \tag{46b}$$

where the prime represents the differentiation with respect to τ. When $\varepsilon = 0$, systems (46a) and (46b) become

$$h' = -\frac{1}{2}\mu I_r + f_0 I_r \sin 2\phi, \tag{47a}$$

$$\phi' = 3\beta_3 I_r h. \tag{47b}$$

Systems (47a) and (47b) are a Hamiltonian system with the Hamiltonian

$$\widehat{H}_D = -\frac{1}{2}\mu I_r \phi - \frac{1}{2}f_0 I_r \cos 2\phi - \frac{3}{2}\beta_3 I_r h^2. \tag{48}$$

A simple calculation indicates that systems (47a) and (47b) have two singular points expressed by

$$P_0 = (0, \phi_c) = \left(0, \frac{1}{2}\arcsin\frac{\mu}{2f_0}\right), \tag{49a}$$

$$Q_0 = (0, \phi_s) = \left(0, \frac{1}{2}\pi - \frac{1}{2}\arcsin\frac{\mu}{2f_0}\right). \tag{49b}$$

It is known that if $6\beta_3 f_0 I_r^2 \cos 2\phi_c < 0$, the singular point P_0 is a center point. And if $6\beta_3 f_0 I_r^2 \cos 2\phi_s > 0$, the singular point Q_0 is a saddle connected to itself by a homoclinic orbit. Figure 2(a) shows the phase portrait of systems (47a) and (47b). It is observed that, for sufficiently small parameter ε, the singular point Q_0 still remains a hyperbolic saddle point Q_ε, while for small perturbations, the singular point P_0 changes to a hyperbolic sink P_ε, see Figure 2(b) for the phase portrait of perturbed systems (46a) and (46b).

On the basis of equation (48), at $h = 0$, the basin of the attractor for $\phi_{\min}$ can be estimated as follows:

$$-\frac{1}{2}\mu I_r \phi_{\min} - \frac{1}{2}f_0 I_r \cos 2\phi_{\min} = -\frac{1}{2}\mu I_r \phi_s - \frac{1}{2}f_0 I_r \cos 2\phi_s. \tag{50}$$

Substituting ϕ_s in (49a) and (49b) into (50) yields

$$\phi_{\min} + \frac{f_0}{\mu}\cos 2\phi_{\min} = \frac{1}{2}\pi - \frac{1}{2}\arcsin\frac{\mu}{2f_0} - \frac{\sqrt{4f_0^2 - \mu^2}}{2\mu}. \tag{51}$$

The neighborhood of I_r is defined as

$$A_\varepsilon = \left\{(z, I, \phi) \mid z = 0, |I - I_r| < \sqrt{\varepsilon}\,C,\ 0 \le \phi \le 2\pi\right\}, \tag{52}$$

where the constant C is sufficiently large so that the unperturbed homoclinic orbit is enclosed within the annulus.

4.2. The Existence of Multipulse Homoclinic Orbits. Based on the results obtained by Haller and Wiggins [20], the dissipative energy-difference function is of the form

$$\begin{aligned} \Delta^n \widehat{H}_D(\phi) = {} & \widehat{H}_D(h, \phi + n\triangle\phi) - \widehat{H}_D(h, \phi) \\ & - \sum_{i=1}^{n}\int_{-\infty}^{+\infty}\langle DH, g\rangle\big|_{(z_1(T_1), z_2(T_1))}\mathrm{d}T_1, \end{aligned} \tag{53}$$

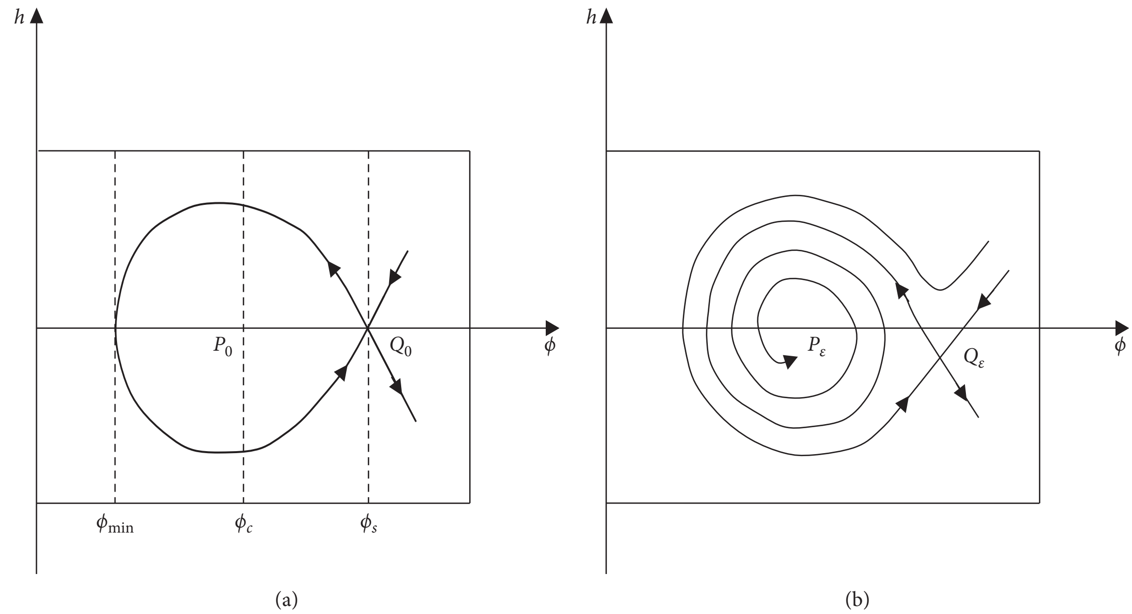

FIGURE 2: Dynamics on the normally hyperbolic manifold: (a) the unperturbed case; (b) the perturbed case.

where

$$\begin{aligned}&\widehat{H}_D(h,\phi+n\Delta\phi)-\widehat{H}_D(h,\phi)\\&\quad=-\frac{1}{2}\mu I_r n\Delta\phi-\frac{1}{2}f_0 I_r\left[\cos(2\phi+2n\Delta\phi)-\cos 2\phi\right],\end{aligned}\tag{54}$$

and A represents the region contained between a pair of homoclinic orbits in the (z_1, z_2) plane, ∂A_l is the boundary of A, and $\Delta\phi$ denotes the phase difference given in (43). The third term in (53) can be calculated as follows:

$$\sum_{i=1}^{n}\int_{-\infty}^{+\infty}\langle DH,g\rangle|_{(z_1(T_1),z_2(T_1))}\mathrm{d}T_1=-\frac{2n\mu\xi_1}{3\alpha_5}\Delta\phi-\frac{1}{2}\mu I_r^2 n\Delta\phi.\tag{55}$$

Thus, the dissipative energy-difference function becomes

$$\begin{aligned}\Delta^n\widehat{H}_D(\phi)&=-\frac{1}{2}f_0 I_r\left[\cos(2\phi+2n\Delta\phi)-\cos 2\phi\right]+\frac{2n\mu\xi_1}{3\alpha_5}\Delta\phi\\&\quad+\frac{1}{2}n\mu I_r(I_r-1)\Delta\phi\\&=f_0 I_r\sin(2\phi+n\Delta\phi)\sin(n\Delta\phi)+\frac{2n\mu\tilde{\xi}_1}{3\alpha_5}\Delta\phi,\end{aligned}\tag{56}$$

where $\tilde{\xi}_1=\xi_1+(3/4)\alpha_5 I_r(I_r-1)$. A dissipation factor is defined as $d=(\mu/f_0)$. Equation (56) can then be rewritten in the following form:

$$\Delta^n\widehat{H}_D(\phi)=f_0\left[I_r\sin(2\phi+n\Delta\phi)\sin(n\Delta\phi)+\frac{2n\tilde{\xi}_1 d}{3\alpha_5}\Delta\phi\right].\tag{57}$$

The zeros of $\Delta^n\widehat{H}_D(\phi)$ can be achieved by solving the following equation:

$$\sin(2\phi+n\Delta\phi)=-\frac{2n\tilde{\xi}_1 d\Delta\phi}{3\alpha_5 I_r\sin(n\Delta\phi)}.\tag{58}$$

The upper bound of the dissipation factor d is derived from equation (58):

$$d<d_{\max}=\left|\frac{3\alpha_5 I_r}{2n\tilde{\xi}_1}\right|\left|\frac{\sin(n\Delta\phi)}{\Delta\phi}\right|.\tag{59}$$

According to (59), it is found that, for small dissipative effects $d<1$, the following upper bound on the pulse numbers is obtained:

$$n<n_{\max}=\left|\frac{3\alpha_5 I_r}{2d\tilde{\xi}_1\Delta\phi}\right|,\tag{60}$$

which means that the homoclinic tree is finite even for arbitrarily small dissipation. The result in equation (60) also indicates that the upper bound $n_{\max}$ is inversely proportional to the dissipation factor d. We now identify zeros of the energy-difference function $\Delta^n\widehat{H}_D(\phi)$ in the interval $[-(\pi/2),(\pi/2)]$. From (57), we find that, for any n satisfying

$$\begin{gathered}n\Delta\phi\neq l\pi,\\ l\in Z,\end{gathered}\tag{61}$$

the zeros of $\Delta^n\widehat{H}_D(\phi)$ in $[-(\pi/2),(\pi/2)]$ are

$$\phi_{-,1}^n=\frac{\pi}{2}-\left[\frac{1}{2}n\Delta\phi+\varphi\right]\bmod\pi,\tag{62a}$$

$$\phi_{-,2}^n=\frac{\pi}{2}-\left[\frac{1}{2}\pi+\frac{1}{2}n\Delta\phi-\varphi\right]\bmod\pi,\tag{62b}$$

where $\varphi=-(1/2)\arcsin(2n\tilde{\xi}_1 d\Delta\phi/3\alpha_5 I_r\sin(n\Delta\phi))$. Define a set that contains all transverse zeros of $\Delta^n\widehat{H}_D(\phi)$ as

$$Z_-^n = \left\{(h,\phi) \mid \Delta^n \widehat{H}_D(\phi) = 0, D_\phi \Delta^n \widehat{H}_D(\phi) \neq 0\right\}. \tag{63}$$

It is easy to know that both zeros are transverse under condition (61). We now need to introduce the two additional angles

$$\phi_{+,1}^n = \left[\phi_{-,1}^n + n\Delta\phi\right] \bmod 2\pi, \tag{64a}$$

$$\phi_{+,2}^n = \left[\phi_{-,2}^n + n\Delta\phi\right] \bmod 2\pi, \tag{64b}$$

and utilize them to construct the two sets of transverse zeros of $\Delta^n \widehat{H}_D(\phi)$ as

$$Z_-^n = \left\{(h,\phi) \mid \phi \in \left\{\phi_{-,1}^n, \phi_{-,2}^n\right\}\right\}, \quad n \geq 1, \tag{65a}$$

$$Z_+^n = \left\{(h,\phi) \mid \phi \in \left\{\phi_{+,1}^n, \phi_{+,2}^n\right\}\right\}, \quad n \geq 1. \tag{65b}$$

Consider a domain $S_0 \in A_\varepsilon$ enclosed inside the homoclinic orbit of (47a) and (47b) located in the interval $\phi \in [-(\pi/2), (\pi/2)]$. The periodic orbits in S_0 are classified according to their pulse numbers, see Figure 3. Note that, under condition (61), all internal orbits outside S_0 intersect Z_-^1 transversally. Thus, for any periodic or homoclinic orbit γ outside S_0, the pulse number is $N(\gamma) = 1$. Define the energy sequence

$$h_0 = \widehat{H}_D(0,\phi_s) = -\frac{1}{2}\mu I_r\left(\frac{\pi}{2} - \frac{1}{2}\arcsin\frac{d}{2}\right) + \frac{1}{4}f_0 I_r\sqrt{4-d^2}, \tag{66a}$$

$$h_n = \min\left[\widehat{H}_D\left(0,\phi_{-,1}^n\right), \widehat{H}_D\left(0,\phi_{-,2}^n\right)\right], \tag{66b}$$

such that h_n provides the energy level related to an orbit closer to the center. Define the open set of internal orbits in S_0 as

$$\begin{aligned} &A_0 = \varnothing, \\ &A_n = \left\{(h,\phi) \in S_0 \mid \widehat{H}_D(h,\phi) > h_n\right\}, \quad n \geq 1. \end{aligned} \tag{67}$$

The pulse sequence is then defined as

$$\begin{aligned} &N_1 = 1, \\ &N_k = \min\left\{n \in Z^+ \mid n > N_{k-1}, h_n < h_{N_{k-1}}\right\}, \quad k \geq 2. \end{aligned} \tag{68}$$

Since the energy of the periodic orbits in S_0 decreases monotonically with the orbits shrinking to the center, we necessarily have

$$A_{N_1} \subset A_{N_2} \subset \cdots A_{N_k} \subset \cdots. \tag{69}$$

The layer sequence is defined as

$$L_{N_k} = \mathrm{Int}\left(\frac{A_{N_k}}{A_{N_{k-1}}}\right), \tag{70}$$

where $\mathrm{Int}(\cdot)$ denotes the interior of a set. And the construction of the layer sequence is shown in Figure 3. We can easily see that all these sequences defined above are finite by (60). For any periodic orbit $\gamma \in S_0$, the pulse number is $N(\gamma) = N_k$. As illustrated in Figure 3, the layer radii are defined as

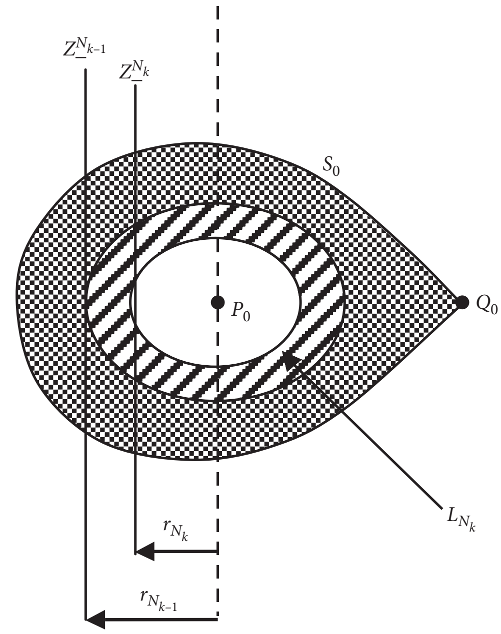

Figure 3: The construction of the layer sequence for (47a) and (47b).

$$r_{N_k} = \min\left[\left|\phi_c - \phi_{-,1}^{N_k}\right|, \left|\phi_c - \phi_{-,2}^{N_k}\right|\right]. \tag{71}$$

A recursive algorithm for the calculation of the distribution of pulse numbers and the layer radii is implemented on a computer. For different values of the dissipation factor d, we obtain the corresponding pulse diagrams and layer radius diagrams as a function of the phase shift $\Delta\phi$ for $N_k < 20$, illustrated in Figures 4 and 5. As can be seen in Figure 4, the horizontal line segments at each level N_k identify that an infinity of N_k-pulse orbits exist for all values of the phase shift in the interval below that line. Besides, the diagrams in Figure 5 exhibit a gradual breakup of the homoclinic tree as d is increased. This observation means that the system parameters have a vital effect on the distribution of the pulse numbers and the layer radii.

We now detect the existence of the multipulse Shilnikov-type orbits based on Theorem 4.5 in [20]. Note that the sinks of (46a) and (46b) become the centers of (47a) and (47b). Therefore, systems (47a) and (47b) have a nondegenerate equilibrium

$$P_0 \equiv (h_c, \phi_c) = (0, \phi_c) = \left(0, \frac{1}{2}\arcsin\frac{d}{2}\right). \tag{72}$$

The values of $(d, \Delta\phi, N)$ for which the center P_0 falls in the zero set Z_-^n given in (63) must be determined, that is,

$$-\frac{1}{2}I_r\left[\cos\left(\arcsin\frac{d}{2} + 2N\Delta\phi\right) - \cos\left(\arcsin\frac{d}{2}\right)\right] + \frac{2N\widetilde{\xi}_1 d\Delta\phi}{3\alpha_5} = 0, \tag{73}$$

which yields

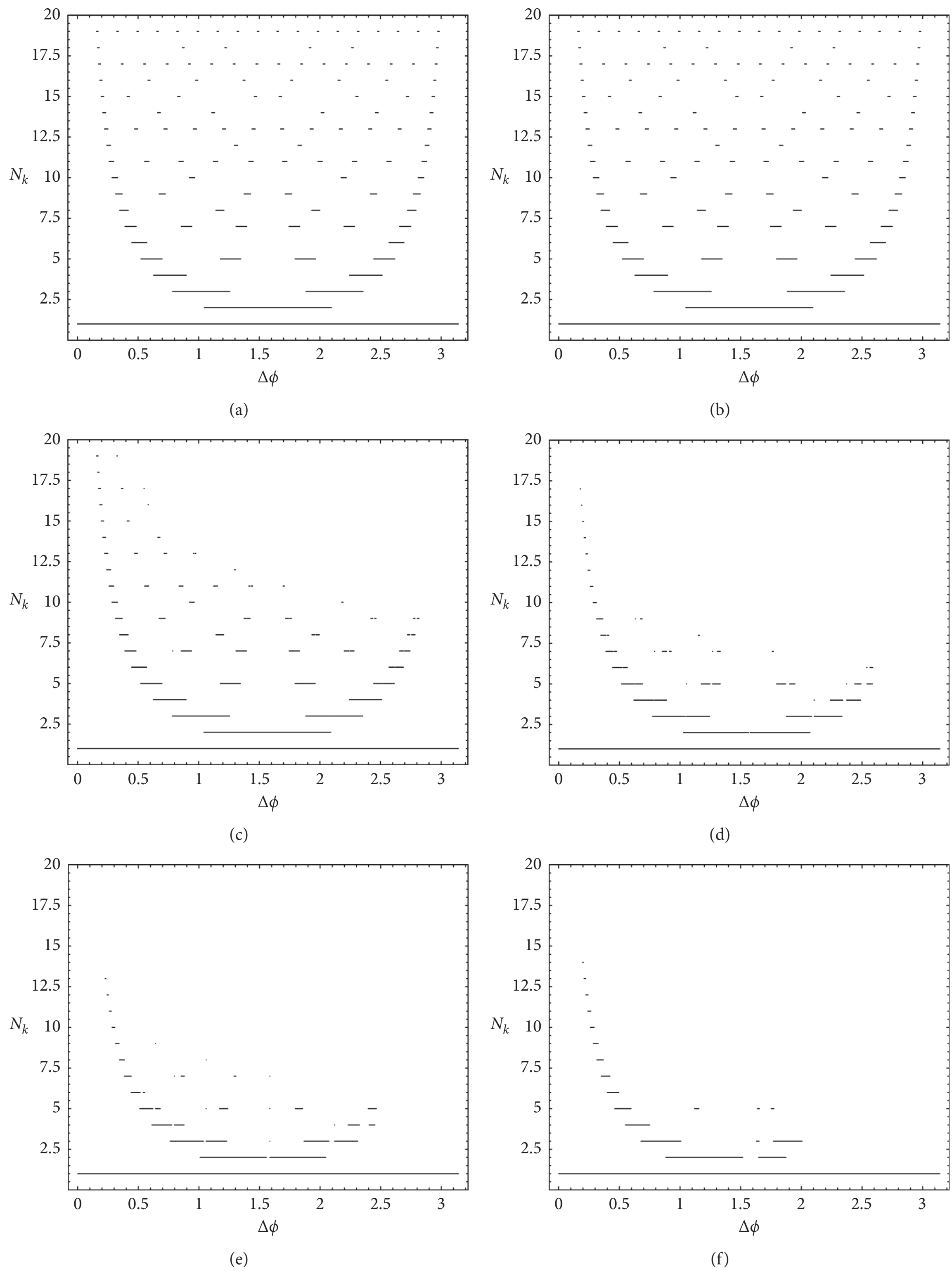

FIGURE 4: The pulse sequence as a function of the phase shift $((\tilde{\xi}_1/\alpha_5 I_r) = (2/15))$. (a) $d = 0$. (b) $d = 10^{-5}$. (c) $d = 0.01$. (d) $d = 0.05$. (e) $d = 0.1$. (f) $d = 0.4$.

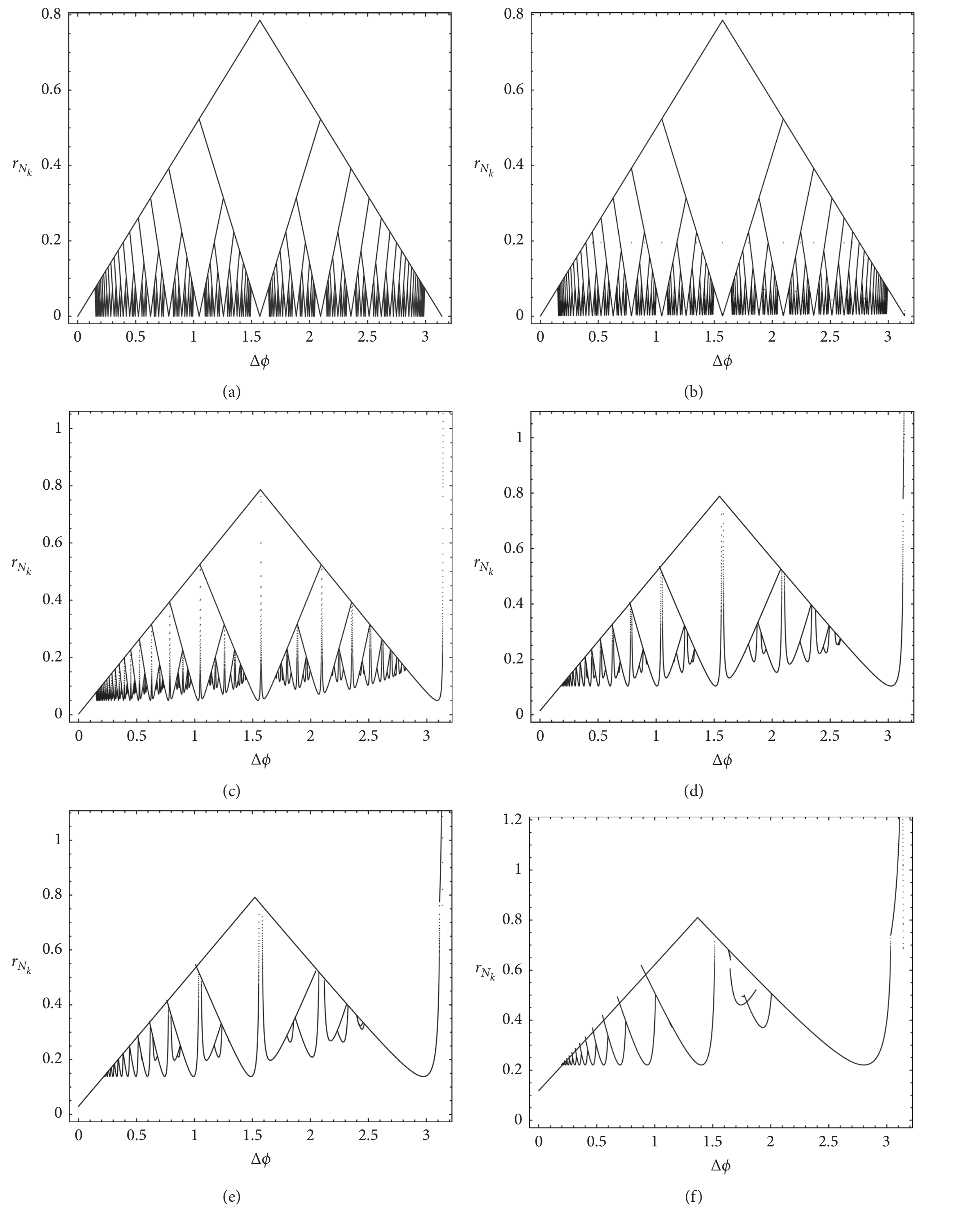

Figure 5: The layer radius sequence as a function of the phase shift $((\widetilde{\xi}_1/\alpha_5 I_r) = (2/15))$. (a) $d = 0$. (b) $d = 10^{-5}$. (c) $d = 0.01$. (d) $d = 0.05$. (e) $d = 0.1$. (f) $d = 0.4$.

$$\sqrt{4-d^2}\left[\cos(2N\Delta\phi)-1\right] = d\left[\sin(2N\Delta\phi)+\frac{8N\tilde{\xi}_1\Delta\phi}{3\alpha_5 I_r}\right]. \tag{74}$$

Solving (74), the dissipation factor d is obtained as

$$d = \frac{2\left[1-\cos(2N\Delta\phi)\right]}{\sqrt{\left[1-\cos(2N\Delta\phi)\right]^2+\left[\sin(2N\Delta\phi)+\left(8N\tilde{\xi}_1\Delta\phi/3\alpha_5 I_r\right)\right]^2}}. \tag{75}$$

The result is only valid when

$$\Delta\phi \neq \frac{m\pi}{N}, \quad m \in Z. \tag{76}$$

It is also necessary to prove the nondegeneracy condition

$$D_d\left\{-\frac{1}{2}I_r\left[\cos\left(\arcsin\frac{d}{2}+2N\Delta\phi\right)-\cos\left(\arcsin\frac{d}{2}\right)\right]+\frac{2N\tilde{\xi}_1 d\Delta\phi}{3\alpha_5}\right\} \neq 0, \tag{77}$$

whenever (74) and (76) hold. Carrying out the differentiation in expression (74), we find that (77) fails to be satisfied when

$$-d\left[\cos(2N\Delta\phi)-1\right] = \sqrt{4-d^2}\left[\sin(2N\Delta\phi)+\frac{8N\tilde{\xi}_1\Delta\phi}{3\alpha_5 I_r}\right]. \tag{78}$$

It is easy to see that equations (74) and (78) cannot hold simultaneously under condition (76). Thus, nondegeneracy condition (77) holds. We now have to guarantee that the landing point of any N-pulse orbit taking off from a slow sink lies in the domain of attraction of a sink on A_ε. To verify it, we consider the point in the interval $[-(\pi/2), (\pi/2)]$ and is $k\pi$ apart from the approximate landing point $\phi_c + N\Delta\phi$. The ϕ-coordinate of this point is calculated as

$$\phi_*^N = \phi_s + \left[\phi_c + N\Delta\phi - \phi_s\right] \bmod \pi, \tag{79}$$

in which we recall that

$$\phi_c = \frac{1}{2}\arcsin\frac{d}{2}, \tag{80a}$$

$$\phi_s = \frac{\pi}{2}-\frac{1}{2}\arcsin\frac{d}{2}. \tag{80b}$$

If $\phi_*^N > \phi_s$, we redefine ϕ_*^N by subtracting π. The main purpose here is to achieve $k\pi$ translation of the landing point which is the closest to the saddle point ϕ_s in the interval $[-(\pi/2), (\pi/2)]$. We require that

$$\widehat{H}_D\left(0,\phi_*^N\right) < \widehat{H}_D\left(0,\phi_s\right), \tag{81}$$

or, equivalently, that

$$\cos 2\phi_*^N - \cos 2\phi_s > d\left(\phi_s - \phi_*^N\right), \tag{82}$$

to make sure that the projection of landing points falls in the domain of attraction of one of the sinks.

Based on the above analysis, the results in this section give rise to the following theorem.

Theorem 1. *For any integer $N \geq 1$, there exists a positive number $\varepsilon_0(N) > 0$ and a finite union C_N of codimension-one surfaces in the $(\tilde{\xi}_1, \alpha_5, \mu, f_0, \varepsilon) \in C_N$ parameter space near the set satisfying $0 < d < 1$, (75), and (82) such that, for any $(\tilde{\xi}_1, \alpha_5, \mu, f_0, \varepsilon) \in C_N$ and $0 < \varepsilon < \varepsilon_0(N)$, the following conclusions hold:*

(1) If the integer

$$Q = \mathrm{INT}\left[\frac{1}{2}+\frac{N\Delta\phi+\arcsin(d/2)}{\pi}\right], \tag{83}$$

is even, then each of the saddle-focus-type equilibria contained in the slow manifold A_ε admits two generalized Shilnikov-type homoclinic orbits. If Q is odd, then there exist two cycles of Shilnikov-type heteroclinic orbits connecting the two saddle-foci to each other. In both cases, the N-pulse orbits form pairs which are symmetric with respect to the subspace $(z_1, z_2) = (0, 0)$.

(2) There exists an open set of parameters containing C_N for which system (26) admits Smale horseshoes in its dynamics.

5. Numerical Simulations

In order to verify the analytical predictions, we choose systems (13a)–(13d) to perform numerical simulations. The fourth-order Runge–Kutta algorithm is employed to indicate the existence of the multipulse Shilnikov-type homoclinic orbits and chaotic motions in the CNT-reinforced composite plate. Figure 6 is obtained to show that there exist multipulse chaotic motions for the CNT-reinforced composite plate. In Figure 6, the parameters and initial conditions are selected as $\mu = 0.05$, $\sigma_1 = -1.86$, $\sigma_2 = 1.5$, $\alpha_1 = 7.2$, $\alpha_2 = -10.8$, $\alpha_3 = -3.9$, $\alpha_4 = 11.6$, $\alpha_5 = 15$, $\beta_2 = -4.78$, $\beta_3 = -4$, $\beta_4 = 5$, $\beta_5 = -7.18$, $f_0 = 12.235$, $(x_1, x_2, x_3, x_4) = (0.105, -0.101, -0.013, -0.506)$, and the phase shift at $I = I_r = \sqrt{-(2\sigma_2/3\beta_3)} = (1/2)$ is $\Delta\phi = 2.37$. We choose the pulse number $N = 4$; then, (75) gives $d = (\mu/f_0) = 0.00409$. Using equations (79) and (80a) and (80b), we have $\phi_*^N = 3.199$, $\phi_s = 1.569$, $\cos 2\phi_*^N - \cos 2\phi_s = 1.993$, and $d(\phi_s - \phi_*^N) = -0.067$. Obviously, condition (82) holds, which implies that the chaotic motion presented in Figure 6 is multipulse Shilnikov-type chaotic motion.

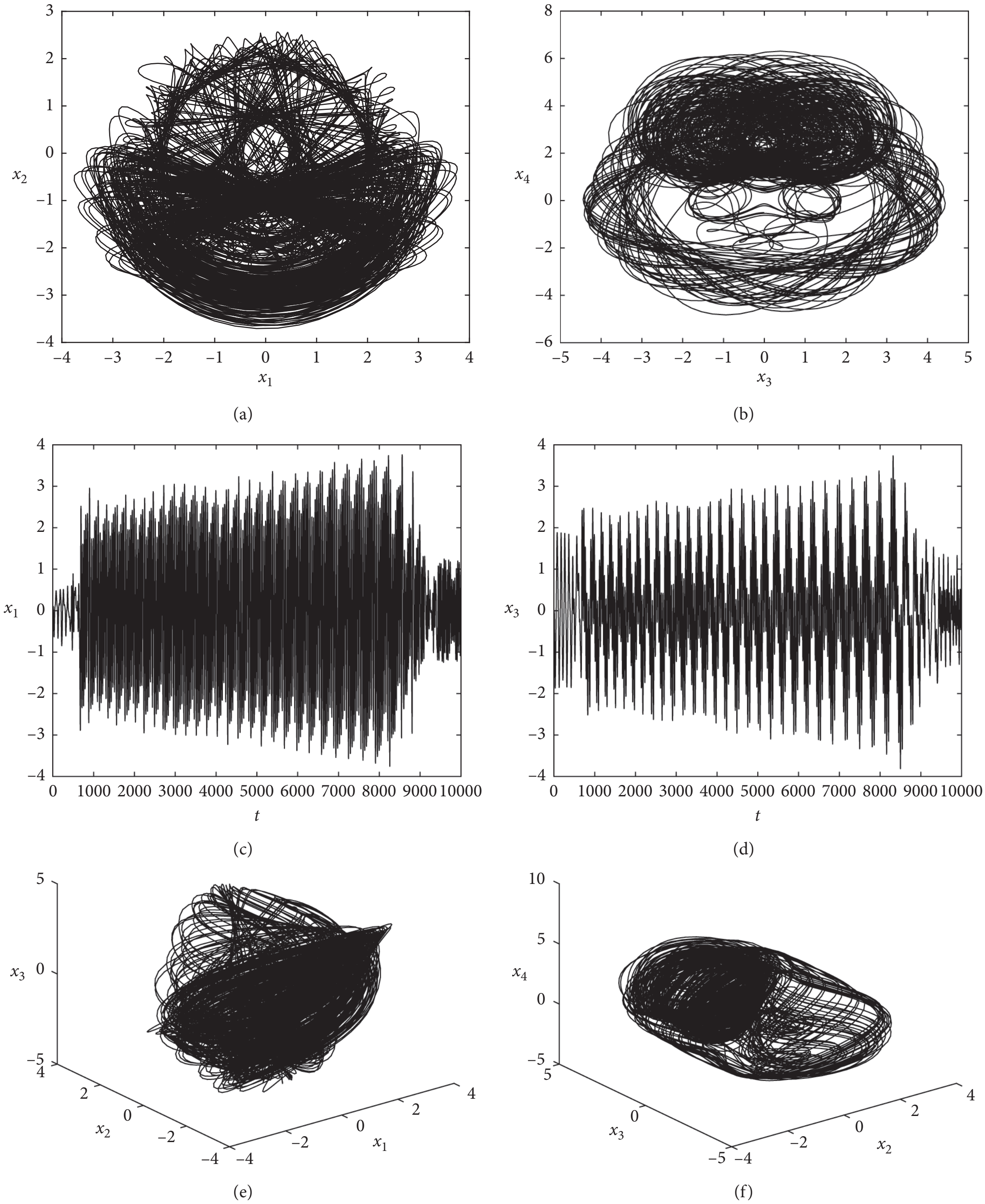

Figure 6: The multipulse chaotic motion obtained based on equation (13): (a) the phase portrait on the plane (x_1, x_2), (b) the phase portrait on the plane (x_3, x_4), (c) the waveform on the plane (t, x_1), (d) the waveform on the plane (t, x_3), (e) the phase portraits in the three-dimensional space (x_1, x_2, x_3), and (f) the phase portraits in the three-dimensional space (x_2, x_3, x_4).

6. Conclusions

In this paper, the multipulse homoclinic orbits and chaotic dynamics of a CNT-reinforced composite plate under combined in-plane and transverse excitations are studied. The method of multiple scales is adopted to acquire the averaged equations in the case of 1 : 1 internal resonance, principal parametric resonance, and 1/2 subharmonic resonance. On the basis of the averaged equations obtained, the normal form theory is employed to derive the expressions of normal form associated with a double zero and a pair of pure imaginary eigenvalues. The energy-phase method proposed by Haller and Wiggins [20] is utilized to detect the presence of the multipulse homoclinic orbits and chaotic dynamics for the resonant case. As the trajectory of motion comes close to the sink point P_ε, every Shilnikov-type orbit takes off again and repeats this similar motion in the full four-dimensional phase space and eventually leads to the multipulse Shilnikov-type orbits. Our analysis in Section 4 also indicates that the multipulse Shilnikov-type orbits depend on the system parameters and dissipative perturbations. It is known that the existence of multipulse Shilnikov-type orbits implies the existence of chaos in the sense of Smale horseshoes. Homoclinic trees are presented to describe the repeated bifurcations of multipulse solutions. From the diagrams, we can see a gradual breakup of the homoclinic tree with the increase of the dissipation factor. This observation denotes that the damping coefficient and system parameters affect the distribution of the pulse numbers and the layer radii. The analytical results obtained here are extensions of those appearing in [19].

To confirm the theoretical results, numerical simulations are applied to examine the chaotic dynamics of the CNT-reinforced composite plate. The numerical results demonstrate that there exist multipulse homoclinic orbits and chaotic dynamics in systems (13a)–(13d) when the conditions are satisfied. As we all know, under certain conditions, the multipulse chaotic motions in the averaged equations can result in the multipulse amplitude-modulated chaotic vibrations in the original system, which indicates the existence of multipulse chaotic dynamics in the CNT-reinforced composite plate. The research in this paper provides a detailed explanation of the multipulse jumping behaviors for the CNT-reinforced composite plate under combined in-plane and transverse excitations. It is established simultaneously that the damping coefficient and system parameters have a significant influence on the nonlinear dynamics of the CNT-reinforced composite plate. Therefore, as mentioned above, the nonlinear dynamic behaviors of the CNT-reinforced composite plate can be controlled by varying the system parameters.

Data Availability

The data used to support the findings of this study are available from the corresponding author upon request.

Conflicts of Interest

The authors declare no conflicts of interest.

Acknowledgments

This research was supported by the National Natural Science Foundation of China (11872201, 11572148, and 11772148), the National Research Foundation for the Doctoral Program of Higher Education of China (20133218110025), the Fundamental Research Funds for the Central Universities (NS2017046), and the Natural Science Research Project for College and University of Anhui Province (KJ2018A0048).

References

[1] G. Formica, W. Lacarbonara, and R. Alessi, "Vibrations of carbon nanotube-reinforced composites," *Journal of Sound and Vibration*, vol. 329, no. 10, pp. 1875–1889, 2010.

[2] P. Zhu, Z. X. Lei, and K. M. Liew, "Static and free vibration analyses of carbon nanotube-reinforced composite plates using finite element method with first order shear deformation plate theory," *Composite Structures*, vol. 94, no. 4, pp. 1450–1460, 2012.

[3] Z.-X. Wang and H.-S. Shen, "Nonlinear dynamic response of nanotube-reinforced composite plates resting on elastic foundations in thermal environments," *Nonlinear Dynamics*, vol. 70, no. 1, pp. 735–754, 2012.

[4] P. Malekzadeh and Y. Heydarpour, "Mixed Navier-layerwise differential quadrature three-dimensional static and free vibration analysis of functionally graded carbon nanotube reinforced composite laminated plates," *Meccanica*, vol. 50, no. 1, pp. 143–167, 2015.

[5] Y. Kiani, "Free vibration of carbon nanotube reinforced composite plate on point Supports using Lagrangian multipliers," *Meccanica*, vol. 52, no. 6, pp. 1353–1367, 2017.

[6] M. Rafiee, X. Q. He, and K. M. Liew, "Non-linear dynamic stability of piezoelectric functionally graded carbon nanotube-reinforced composite plates with initial geometric imperfection," *International Journal of Non-linear Mechanics*, vol. 59, pp. 37–51, 2014.

[7] A. Alibeigloo and K. M. Liew, "Thermoelastic analysis of functionally graded carbon nanotube-reinforced composite plate using theory of elasticity," *Composite Structures*, vol. 106, pp. 873–881, 2013.

[8] A. Alibeigloo and A. Emtehani, "Static and free vibration analyses of carbon nanotube-reinforced composite plate using differential quadrature method," *Meccanica*, vol. 50, no. 1, pp. 61–76, 2015.

[9] L. W. Zhang, W. H. Liu, and K. M. Liew, "Geometrically nonlinear large deformation analysis of triangular CNT-reinforced composite plates," *International Journal of Non-linear Mechanics*, vol. 86, pp. 122–132, 2016.

[10] J. Zhang and S. Li, "Dynamic buckling of FGM truncated conical shells subjected to non-uniform normal impact load," *Composite Structures*, vol. 92, no. 12, pp. 2979–2983, 2010.

[11] E. Bagherizadeh, Y. Kiani, and M. R. Eslami, "Mechanical buckling of functionally graded material cylindrical shells surrounded by Pasternak elastic foundation," *Composite Structures*, vol. 93, no. 11, pp. 3063–3071, 2011.

[12] J. Sun, X. Xu, C. W. Lim, and W. Qiao, "Accurate buckling analysis for shear deformable FGM cylindrical shells under axial compression and thermal loads," *Composite Structures*, vol. 123, pp. 246–256, 2015.

[13] A. J. M. Ferreira, "A formulation of the multiquadric radial basis function method for the analysis of laminated composite plates," *Composite Structures*, vol. 59, no. 3, pp. 385–392, 2003.

[14] O. Civalek, "Free vibration analysis of composite conical shells using the discrete singular convolution algorithm," *Steel and Composite Structures*, vol. 6, no. 4, pp. 353–366, 2006.

[15] O. Civalek, "Linear vibration analysis of isotropic conical shells by discrete singular convolution (DSC)," *Structural Engineering and Mechanics*, vol. 25, no. 1, pp. 127–130, 2007.

[16] O. Civalek, "Vibration analysis of conical panels using the method of discrete singular convolution," *Communications in Numerical Methods in Engineering*, vol. 24, no. 3, pp. 169–181, 2008.

[17] Ö. Civalek and M. H. Acar, "Discrete singular convolution method for the analysis of Mindlin plates on elastic foundations," *International Journal of Pressure Vessels and Piping*, vol. 84, no. 9, pp. 527–535, 2007.

[18] B. Akgoz and O. Civalek, "Nonlinear vibration analysis of laminated plates resting on nonlinear two-parameters elastic

foundations," *Steel & Composite Structures*, vol. 11, no. 5, pp. 403–421, 2011.

[19] X. Y. Guo and W. Zhang, "Nonlinear vibrations of a reinforced composite plate with carbon nanotubes," *Composite Structures*, vol. 135, pp. 96–108, 2016.

[20] G. Haller and S. Wiggins, "*N*-pulse homoclinic orbits in perturbations of resonant Hamiltonian systems," *Archive for Rational Mechanics and Analysis*, vol. 130, no. 1, pp. 25–101, 1995.

[21] R. Camassa, G. Kovačič, and S.-K. Tin, "A Melnikov method for homoclinic orbits with many pulses," *Archive for Rational Mechanics and Analysis*, vol. 143, no. 2, pp. 105–193, 1998.

[22] W. Zhang, M. H. Yao, and J. H. Zhang, "Using the extended Melnikov method to study the multi-pulse global bifurcations and chaos of a cantilever beam," *Journal of Sound and Vibration*, vol. 319, no. 1-2, pp. 541–569, 2009.

[23] W. Zhang, J. H. Zhang, and M. H. Yao, "The extended Melnikov method for non-autonomous nonlinear dynamical systems and application to multi-pulse chaotic dynamics of a buckled thin plate," *Nonlinear Analysis: Real World Applications*, vol. 11, no. 3, pp. 1442–1457, 2010.

[24] W. Zhang and W. L. Hao, "Multi-pulse chaotic dynamics of six-dimensional non-autonomous nonlinear system for a composite laminated piezoelectric rectangular plate," *Nonlinear Dynamics*, vol. 73, no. 1-2, pp. 1005–1033, 2013.

[25] N. Malhotra, N. Sri Namachchivaya, and R. J. McDonald, "Multipulse orbits in the motion of flexible spinning discs," *Journal of Nonlinear Science*, vol. 12, no. 1, pp. 1–26, 2002.

[26] R. J. McDonald and N. Sri Namachchivaya, "Pipes conveying pulsating fluid near a resonance: global bifurcations," *Journal of Fluids and Structures*, vol. 21, no. 5–7, pp. 665–687, 2005.

[27] M. Yao and W. Zhang, "Multipulse Shilnikov orbits and chaotic dynamics for nonlinear nonplanar motion of a cantilever beam," *International Journal of Bifurcation and Chaos*, vol. 15, no. 12, pp. 3923–3952, 2005.

[28] W. Zhang and M. Yao, "Multi-pulse orbits and chaotic dynamics in motion of parametrically excited viscoelastic moving belt," *Chaos, Solitons & Fractals*, vol. 28, no. 1, pp. 42–66, 2006.

[29] S. B. Li, W. Zhang, and M. H. Yao, "Using energy-phase method to study global bifurcations and Shilnikov type multipulse chaotic dynamics for a nonlinear vibration absorber," *International Journal of Bifurcation and Chaos*, vol. 22, no. 1, Article ID 1250001, 2012.

[30] Y. X. Hao, W. Zhang, J. Yang, and S. B. Li, "Nonlinear dynamics of a functionally graded thin simply-supported plate under a hypersonic flow," *Mechanics of Advanced Materials and Structures*, vol. 22, no. 8, pp. 619–632, 2015.

[31] W. Zhang, F. Wang, and J. W. Zu, "Computation of normal forms for high dimensional non-linear systems and application to non-planar non-linear oscillations of a cantilever beam," *Journal of Sound and Vibration*, vol. 278, no. 4-5, pp. 949–974, 2004.